University of Tehran Press

Online ISSN: 2345-475X

DESERT

Home page: https://jdesert.ut.ac.ir/

Enhanced Groundwater Level Prediction through a Hybrid Multi-Model Approach Using Satellite Data

Jamshid Piri[1], Adnan Sadeghi-Lari[2*], Mohammad Kazemi[2], Narges Kariminejad[3]

[1] Department of Water Engineering, Faculty of Water and Soil, University of Zabol, Zabol, Sistan and Balochestan Province, Iran

[2] Department of Water Science and Engineering, Faculty of Agriculture and Natural Resources, University of Hormozgan, Bandar Abbas, Iran. Email: adnan.sadeghilari@hormozgan.ac.ir

[3] Department of Natural Resources and Environmental Engineering, College of Agriculture, Shiraz University, Shiraz, Iran

Article Info.

Article type:
Research Article

Article history:
Received: 17 Apr. 2026
Received in revised from: 10 Jun. 2026
Accepted: 17 Jun. 2026
Published online: 18 Jun. 2026

Keywords:
Groundwater monitoring,
Satellite data integration,
GMDH-Harmony Search,
Arid region hydrology.

ABSTRACT

This study proposes a novel hybrid modeling framework that integrates satellite-derived data with Group Method of Data Handling (GMDH) models to enhance groundwater level prediction in arid and data-scarce regions, specifically the Kahoorestan Plain in southern Iran. The objectives were: (1) to develop new models suitable for prediction in sparse data regions, (2) to analyze different optimization methods (Genetic Algorithm and Harmony Search) for improving GMDH performance, and (3) to provide trend analysis of groundwater depletion over time and space. Input data included GRACE-JPL gravity data, potential evapotranspiration, TRMM precipitation, temperature, and soil moisture from satellites. Three model variants were applied: standard GMDH, GMDH-GA, and GMDH-HS. The GMDH-HS model outperformed others with 27–39% lower mean error than standard GMDH, achieving R^2 values between 0.82 and 0.94 across 15 observation wells. Decadal forecasts (10-year projections) indicated critical groundwater declines in the eastern region, with an anticipated drop below surface level to -1.851 meters, signaling severe aquifer stress. These findings are essential for developing tailored intervention plans, including zoned extraction policies and early warning systems, for conservation efforts in at-risk areas.

Cite this article: Piri, J., Sadeghi-Lari, A., Kazemi, M., Kariminejad, N. (2026). Enhanced Groundwater Level Prediction through a Hybrid Multi-Model Approach Using Satellite Data. DESERT, 31 (1), DOI: 10.22059/jdesert.2026.108045

DOI: 10.22059/jdesert.2026.108045

Publisher: University of Tehran Press

1. Introduction

Global water security depends heavily on groundwater, which supplies approximately half of the world's drinking water and supports essential agricultural and industrial activities (Mukherjee *et al*., 2021; Yeh *et al*., 2016). In arid and semi-arid regions, groundwater is the primary source for both human consumption and agriculture (El Kenawy, 2024; Rahmani *et al*., 2023; Safa *et al*., 2020), making it central to achieving the United Nations' Sustainable Development Goal 6. However, increasing environmental pressures, climate change, and water scarcity demand sophisticated spatial modeling and monitoring systems to understand and predict aquifer behavior (Sadeghi-Lari *et al*., 2024; Scanlon *et al*., 2023; Uddin *et al*., 2024). Traditional monitoring approaches, while valuable, have proven insufficient for capturing the complex dynamics of modern hydrological systems (Forliano *et al*., 2024; Kotir *et al*., 2024; Rezk *et al*., 2024), necessitating more advanced, real-time analytical tools (Bamal *et al*., 2024).

Satellite-based Earth observation systems have revolutionized groundwater monitoring over the past decade (Dube *et al*., 2023; Kumar and Choudhury, 2024; Lubis *et al*., 2025; Sajib *et al*., 2025). Missions such as GRACE and GRACE-FO provide unprecedented insights into large-scale groundwater storage changes, enabling tracking of aquifer depletion across regional and continental scales (Ibrahim *et al*., 2024). While satellite data offers advantages including continuous spatial coverage and cost-effective acquisition, fully harnessing its potential requires advanced analytical methods. The emergence of machine learning has transformed hydrological modeling, introducing powerful tools for processing complex environmental data (Saha and Pal, 2024; Shams and Muhammad, 2023), and enabling more accurate predictions of groundwater behavior (Tao *et al*., 2022).

Recent progress has focused on hybridizing statistical and machine learning models to overcome the limitations of conventional approaches. Traditional statistical techniques (e.g., time series analysis, regression) have struggled to capture non-linear interactions in groundwater systems, particularly in regions with sparse monitoring networks (Sengupta *et al*., 2022). The integration of remote sensing with ground-based observations has proven effective for groundwater storage assessment, subsidence monitoring, and discharge zone identification (Adams *et al*., 2022; Springer *et al*., 2023). The GMDH represents a significant advancement in modeling complex hydrological systems (Panahi *et al*., 2022; Piri *et al*., 2024). Hybrid models, such as GMDH-HS (Harmony Search), are particularly suited for hydrological applications due to their ability to simultaneously optimize network structure and parameters, effectively capturing non-linear processes like recharge, discharge, and seasonal variability.

This research develops and tests three hybrid models (GMDH, GMDH-GA, and GMDH-HS) for groundwater level prediction, evaluated through quantitative metrics including RMSE, R^2, and MAE, along with spatial analysis of prediction errors. The specific objectives are: (1) to develop new GMDH-based models suitable for prediction in data-scarce regions using satellite data, (2) to analyze the effectiveness of Genetic Algorithm and Harmony Search optimization methods for improving GMDH performance, and (3) to provide decadal trend analysis of groundwater depletion over time and space across 15 observation wells. Southern Iran's Kahoorestan Plain, characterized by arid conditions (aridity index 0.11), low recharge rates, and high susceptibility to over-extraction, presents distinctive water management challenges. This study develops a novel hybrid GMDH framework tailored to these conditions, using multiple satellite-derived datasets and spatial optimization strategies to address data scarcity and enhance prediction accuracy in similar arid aquifers globally.

2. Materials and methods

2.1 Study Area and Satellite Data Processing

The Kahoorestan Plain aquifer, located in northwestern Persian Gulf, Hormozgan Province, southern Iran (27°07′–27°16′N, 55°25′–55°45′E; 273.2 km²), exhibits a hot desert climate (BWh) with mean annual rainfall of 190 mm and potential evapotranspiration exceeding 1700 mm/year, yielding an aridity index (precipitation/PET) of approximately 0.11 (UNEP guidelines) (Sadeghi-Lari *et al*., 2024). These conditions cause slow natural recharge, high evaporation losses, vulnerability to overexploitation, and saltwater intrusion from three directions, with approximately 680 wells supplying drinking and irrigation water across groundwater levels ranging from –7 m (southeast) to +50 m (northwest) (Fig. 1).

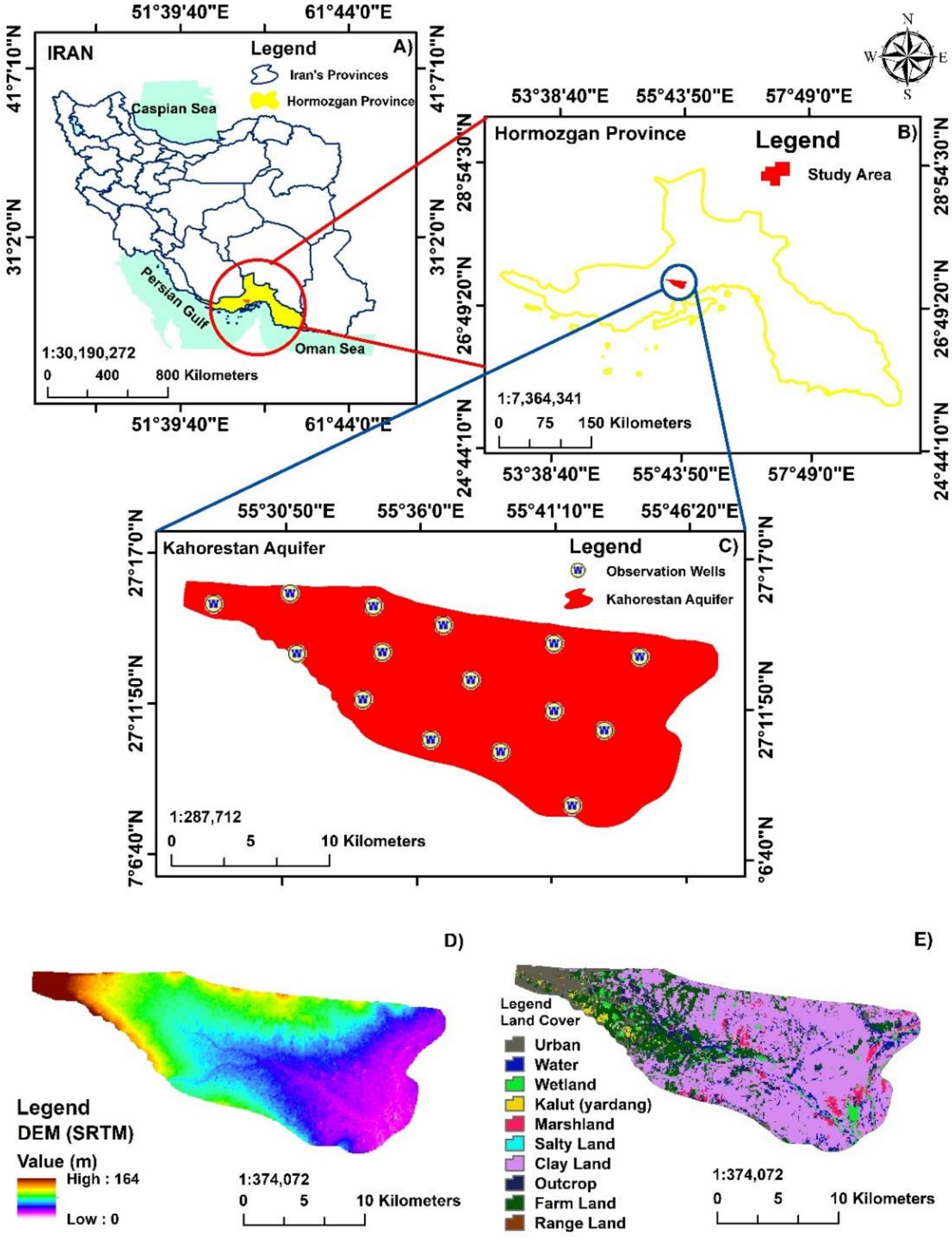

Figure 1. The geographic map of the research area

To capture both direct (precipitation, soil moisture) and indirect (evapotranspiration, vegetation) influences on groundwater levels, satellite-derived parameters including GRACE-JPL gravity data (1°×1°, monthly), TRMM precipitation (0.25°×0.25°, daily), PET, temperature, and soil moisture (0.5°×0.5°, monthly/daily) were selected from a broader dataset (AET, EVI, LST, PDSI, runoff, volumetric soil water at 3m depth). GRACE-JPL provides terrestrial water storage variations, PET monitors atmospheric water demand, temperature affects evaporation and vegetation consumption, and soil moisture tracks vadose zone movement. These multi-resolution datasets underwent harmonization via: (1) monthly temporal aggregation via weighted averaging to match groundwater measurements, (2) bilinear interpolation to 250 m spatial resolution, (3) modified Z-score outlier detection (>3.5 threshold), and (4) temporal interpolation for ~3% missing data. Temporal aggregation mitigated misalignment errors, spatial downscaling enhanced local hydrogeological feature capture, and outlier removal improved training stability. Notably, higher-resolution data (0.25°, e.g., soil moisture, TRMM) yielded approximately 12% lower prediction errors compared to coarse-resolution regions.

2.2. Model Development

2.2.1. GMDH Base Model

The GMDH is a self-organizing algorithm that automatically determines optimal model structure and parameters for complex nonlinear problems (Ivakhnenko, 2020; Ivakhnenko, 1971). Using a multilayer network architecture, GMDH progressively discovers hidden relationships within data, making it particularly effective for hydrological systems where traditional linear methods fail (Xu *et al*., 2021). The algorithm is founded on the Kolmogorov-Gabor polynomial, where each neuron implements a second-order polynomial transfer function (Eq. 1; Table 1) whose coefficients are determined via least squares regression (Zhou *et al*., 2024). Network construction proceeds iteratively: in each layer, all possible pairs of input variables are combined into partial models, with the number of first-layer neurons given by $N = n(n-1)/2$ (FatehiJananloo *et al*., 2024). Model evaluation employs Mean Square Error (MSE, Eq. 2; Table 1) as an external criterion to identify effective partial models while preventing overfitting (Kumar *et al*., 2021). For the Kahoorestan Plain (15 observation wells), inputs include historical groundwater levels and hydrogeological parameters. Model complexity is controlled via a regularization criterion (Eq. 3; Table 1) that balances accuracy against structural parsimony (Dodangeh *et al*., 2020). Training continues until a maximum layer count or minimal improvement threshold is reached, yielding an optimal network that captures underlying patterns without unnecessary complexity.

2.2.2. Rationale for Optimization Algorithm Selection

Two evolutionary methods—Genetic Algorithm (GA) and Harmony Search (HS)—were selected to enhance GMDH performance. GA was chosen for its efficacy in multi-dimensional optimization with multiple local optima; its population-based approach (selection, crossover, mutation) optimizes network structure and parameters while maintaining solution diversity, preventing premature convergence. HS was selected for its balance between global exploration and local exploitation. Inspired by musical improvisation, HS requires fewer function evaluations—advantageous for satellite data processing—and performs better on continuous parameter optimization problems, generating more diverse candidate solutions than GA's pairwise crossover. Both hybrids overcome limitations of fixed-structure networks in capturing spatiotemporal groundwater complexity.

2.2.3. GMDH-GA Hybrid Model

The GMDH-GA model integrates GMDH's self-organizing capabilities with GA's evolutionary optimization (Zhou *et al*., 2024). Each chromosome encodes a complete GMDH configuration as a string of polynomial coefficients (Eq. 4; Table 1) (Khajeh *et al*., 2024). A multi-objective fitness function (Eq. 5; Table 1) balances MSE, model complexity, and structural stability. The algorithm employs tournament selection with elitism, adaptive crossover (Eq. 6; Table 1), and Gaussian mutation with adaptive step size (Eq. 7; Table 1). Performance enhancements include: (i) adaptive layer optimization determining optimal layer count via a regularization criterion (Eq. 8; Table 1); (ii) feature selection probability updated based on relevance and selection frequency (Eq. 9; Table 1); and (iii) adaptive convergence control balancing exploration and exploitation (Eq. 10; Table 1). The GMDH-GA model achieved 15–25% reduction in prediction error across temporal scales, with enhanced nonlinear dynamics capture and improved stability.

2.2.4. GMDH-HS Hybrid Model

The GMDH-HS model combines GMDH's structural learning with Harmony Search's efficient optimization, inspired by musical improvisation (Sabangban *et al*., 2023). Each harmony vector represents a complete set of polynomial coefficients stored in a harmony memory matrix of size HMS (Eq. 11; Table 1). The objective function (Eq. 12; Table 1) integrates MSE (Eq. 2; Table 1), model complexity, and regularization with adaptive weights. Dynamic parameter adjustments govern pitch adjustment rate (PAR, Eq. 13; Table 1), bandwidth (BW, Eq. 14; Table 1), and harmony memory consideration rate (HMCR, Eq. 15; Table 1) over iterations. New harmony vectors are generated either from memory or randomly (Eq. 16; Table 1). Prediction accuracy is evaluated using RMSE (Eq. 17; Table 1) and R^2 (Eq. 18; Table 1). Validation demonstrated 18–30% reduction in mean absolute error, enhanced long-term stability, improved nonlinear handling, and 40% faster convergence compared to GMDH-GA. The model's dynamic adaptation and computational efficiency make it ideal for real-time monitoring in arid regions.

Table 1. Equation, description, and sources of the applied models

Eq.	Equation	Description	Source
(1)	$z = a_0 + a_1x_1 + a_2x_2 + a_3x_1^2 + a_4x_2^2 + a_5x_1x_2$	GMDH neuron transfer function	Zhou *et al*. (2024)
(2)	$MSE = \frac{1}{m}\sum_{i=1}^{m}(y_i - \hat{y}_i)^2$	Mean square error	Kumar *et al*. (2021)
(3)	$\text{Criterion} = MSE + \alpha\frac{p}{n}$	Complexity regulation	Dodangeh *et al*. (2020)
(4)	$\text{Chromosome} = [a_{11}, a_{12}, \dots, a_{mn}]$	GA chromosome encoding	Khajeh *et al*. (2024)
(5)	$\text{Fitness} = w_1 \cdot MSE + w_2 \cdot C + w_3 \cdot S$	Multi-objective fitness function	-
(6)	$\text{Offspring} = \alpha \cdot \text{Parent}_1 + (1-\alpha) \cdot \text{Parent}_2$	Adaptive	-

Eq.	Equation	Description	Source
		crossover	
(7)	$\theta_{new} = \theta_{old} + N(0, \sigma^2)$	Gaussian mutation	-
(8)	$L_{opt} = \arg\min_l [MSE(l) + \lambda C(l)]$	Adaptive layer optimization	-
(9)	$P_s(i) = \beta_1 R(i) + \beta_2 F(i)$	Feature selection probability	-
(10)	$\sigma(t+1) = \sigma(t) \cdot \exp(-k \cdot t/T)$	Adaptive convergence control	-
(11)	$HM = [x_j^i]_{HMS \times N}$	Harmony memory matrix	Sabangban *et al*. (2023)
(12)	$F = MSE + w_1 C + w_2 R$	HS objective function	-
(13)	$PAR(t) = PAR_{min} + (PAR_{max} - PAR_{min}) \cdot \frac{t}{T}$	PAR update	-
(14)	$BW(t) = BW_{max} \cdot \exp\left(\frac{\ln(BW_{min}/BW_{max})}{T} \cdot t\right)$	Bandwidth update	-
(15)	$HMCR(t) = HMCR_{min} + (HMCR_{max} - HMCR_{min}) \cdot \frac{t}{T}$	HMCR update	-
(16)	$x_{new}(j) = \begin{cases} x_{HM}(i,j) & \text{if } r_1 \leq HMCR \\ x_{min}(j) + r_2 \cdot (x_{max}(j) - x_{min}(j)) & \text{otherwise} \end{cases}$	New harmony generation	-
(17)	$RMSE = \sqrt{\frac{1}{n}\sum_{i=1}^{n}(y_i - \hat{y}_i)^2}$	Root mean square error	-
(18)	$R^2 = 1 - \frac{\sum_{i=1}^{n}(y_i - \hat{y}_i)^2}{\sum_{i=1}^{n}(y_i - \bar{y})^2}$	Coefficient of determination	-

2.3. Analysis Approach
2.3.1. Data Preprocessing
Monthly groundwater level readings from 15 observation wells in the Kahoorestan Plain were collected over the period 2008–2022. Inconsistent monitoring resulted in incomplete datasets and irregular outliers. To address these issues, temporal interpolation and statistical normalization were integrated to achieve variable consistency, while a modified Z-score

method enabled accurate identification and handling of extreme values while preserving data integrity.

Min-Max Normalization: Time series data for each observation well were normalized using the min-max scaling method:

$$X_{norm} = \frac{X - X_{min}}{X_{max} - X_{min}} \tag{19}$$

where X_{norm} is the normalized value, and X_{min} and X_{max} are the minimum and maximum values in the dataset, respectively. This normalization scaled all input variables to a uniform range of [0، 1], enhancing model stability and convergence.

Temporal Interpolation for Missing Data: Missing data points, which constituted approximately 3% of the total dataset, were addressed using a temporal interpolation method:

$$X_t = \alpha_1 X_{t-1} + \alpha_2 X_{t+1} \tag{20}$$

where X_t is the interpolated value at time t, and α_1, α_2 are weighting coefficients based on temporal proximity (typically $\alpha_1 = \alpha_2 = 0.5$ for equal weighting).

Outlier Detection: Outlier detection employed the modified Z-score method:

$$M_i = \frac{0.6745 \cdot (X_i - \tilde{X})}{MAD} \tag{21}$$

where MAD is the median absolute deviation, $\tilde{X}$ is the median of the dataset, and values with $| M_i | > 3.5$ were flagged for expert review. This threshold was selected to preserve natural variability while removing erroneous measurements.

2.3.2. Model Training Procedures

The training process implemented a comprehensive approach utilizing **70% of the available data (2008–2018)** for model development. The training procedure was structured to optimize both model parameters and architecture simultaneously. For each model variant (GMDH, GMDH-GA, and GMDH-HS), the training process followed these steps:

Step 1 – Initial Parameter Selection:

- GMDH parameters: $P = [layer_{max}, neuron_{min}, polynomial_{degree}]$
- Training criteria: $MSE_{threshold} = 0.001$

Step 2 – Model Architecture Optimization: The layer-wise training process employed the objective function defined in Equation (12).

Step 3 – Parameter Updates: For each epoch e, parameters were updated according to:

$$\theta_{e+1} = \theta_e - \eta \cdot \nabla J(\theta_e) \tag{22}$$

where η represents the learning rate (dynamically adjusted based on performance improvement), θ_e are the model parameters at epoch e, and $\nabla J(\theta_e)$ is the gradient of the objective function.

2.4. Validation Methods

The validation phase utilized **15% of the dataset** to assess model performance and prevent overfitting. The validation process implemented multiple evaluation criteria:

1. Prediction Accuracy Metrics: Root Mean Square Error (RMSE) and Coefficient of Determination (R^2) were calculated using Equations (17) and (18), respectively.

2. Cross-Validation: k-fold cross-validation ($k = 5$) was implemented to assess model stability across different data subsets. For each fold f, the validation error was computed as:

$$CV_{error} = \frac{1}{5} \sum_{f=1}^{5} E_f \tag{23}$$

where E_f represents the error for fold f, calculated as $E_f = \frac{1}{n_f} \sum_{i=1}^{n_f} (y_i - \hat{y}_i)^2$, and n_f is the number of samples in fold f.

3. Willmott's Index of Agreement (d): This metric balances under-prediction and over-prediction tendencies:

$$d = 1 - \frac{\sum_{i=1}^{n} (y_i - \hat{y}_i)^2}{\sum_{i=1}^{n} (|\hat{y}_i - \bar{y}| + |y_i - \bar{y}|)^2} \quad (24)$$

where y_i is the observed value, $\hat{y}_i$ the predicted value, and $\bar{y}$ the mean of observations. The index ranges between 0 and 1:

$$0 \leq d \leq 1 \quad (25)$$

with values closer to 1 indicating better agreement between predicted and observed values.

3. Results

To analyze groundwater level distributions across multiple wells, three probability distribution functions were considered: The Normal (Gaussian), Lognormal, and Gumbel (Extreme Value Type I) distributions. The Normal distribution was selected because it accurately represents symmetrical data, which is commonly observed in natural phenomena influenced by several independent factors. Groundwater levels typically exhibit skewed distributions with non-negative values, which led to the choice of the Lognormal distribution. The Gumbel distribution function enables researchers to model extreme values, which are crucial in the hydrological analysis of maximum and minimum water levels. To assess the fit of these distributions, three statistical tests were applied: the Kolmogorov-Smirnov (KS) test, the Anderson-Darling (AD) test, and the Chi-Square test. The KS test evaluated the cumulative distribution functions both empirically and theoretically, while the AD test examined the tails of the distribution. The Chi-Square test assessed how well the distribution matched across the entire data spectrum. The comprehensive approach led to the selection of the optimal distribution for each well by analyzing both central tendencies and extreme values, which play a critical role in hydrological management and planning.

Statistical analysis of groundwater levels across 15 wells revealed complex distribution patterns (Fig. 2 and Table 2). Three goodness-of-fit tests (Kolmogorov-Smirnov, Anderson-Darling, and Chi-Square) were employed to evaluate the fit of Normal and Lognormal distributions.

The comparative results demonstrated that the Lognormal distribution provided a superior fit in most cases, particularly for wells exhibiting positively skewed data. There was a good fit for 9 out of 15 wells (60%), which indicates asymmetrical variations in groundwater levels. There was a strong correlation between Well 14 and the Lognormal distribution ($p = 0.092784$).

In three wells (8, 10 and 15), poor fits were observed across all distributions, suggesting complex hydrogeological factors are at play locally. This may include factors such as saline water intrusion, aquifer boundary effects, or localized pumping stress.

Across all wells, Anderson-Darling test values were consistently low (0.0005), illustrating the limitations of conventional distribution models. This implies that while simple distributions may capture general trends, more flexible or site-specific models may be required for wells with anomalous behavior.

As the spatial pattern of distribution correlates with regional hydrogeological characteristics, eastern wells exhibit different statistical characteristics than those in the west.

These findings underscore the importance of site-specific analysis and highlight the potential limitations of conventional distribution models in accurately characterizing groundwater level behavior. More advanced statistical techniques may be necessary for effective groundwater management and planning. The dominance of Lognormal distributions for groundwater levels in 60% of the wells suggests that the system exhibits positive skewness, possibly due to high variability in recharge and extraction rates. The poor fit in wells 8, 10, and 15 may reflect local hydrogeological complexities, such as the proximity to saline intrusion zones or structural heterogeneities in the aquifer.

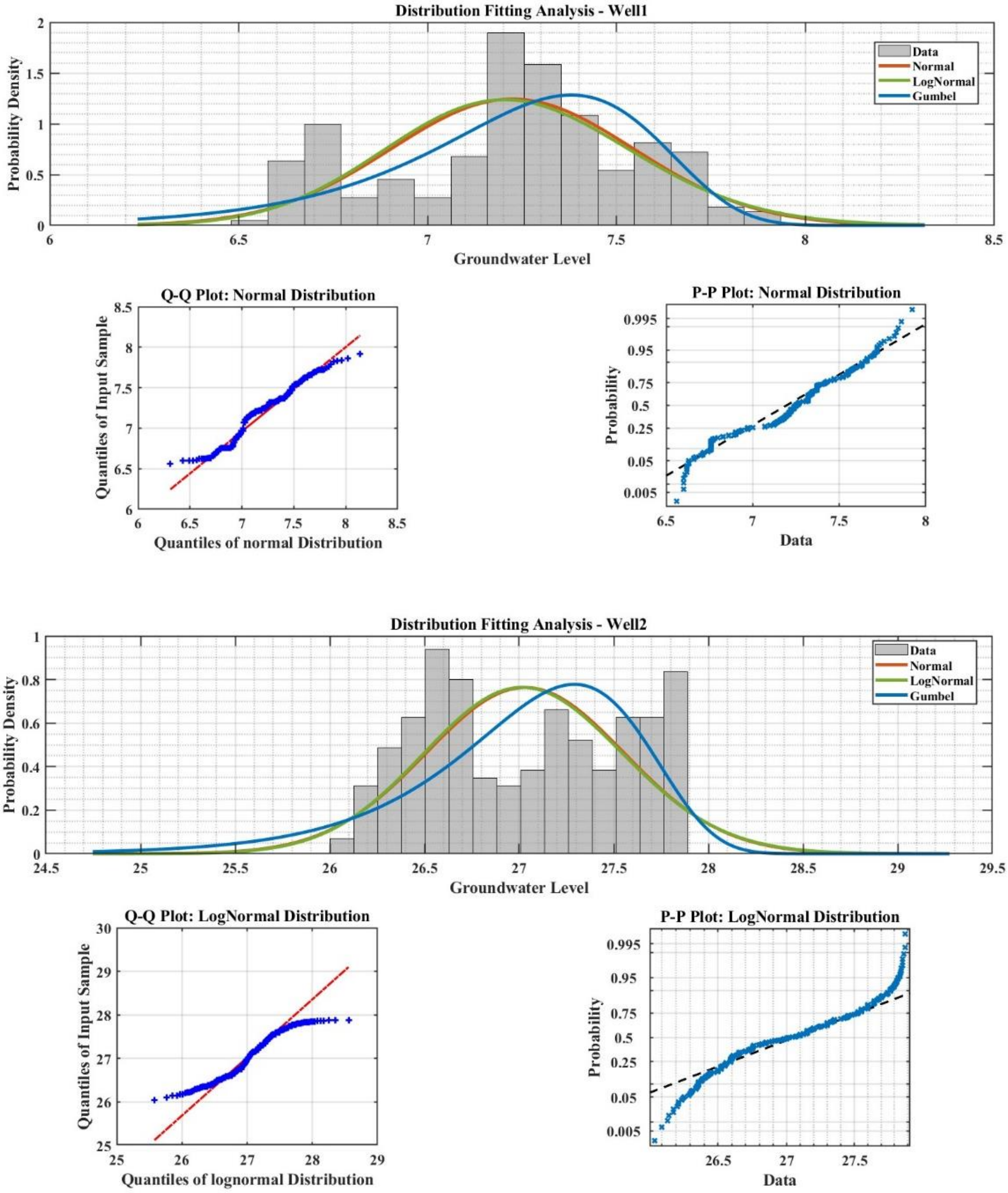

Figure 2. Distribution Fitting Comparison- well1, well2, well3, well4, well5, well6, well7, well8,

well9, well10, well11, well12, well13, well14, and well15.

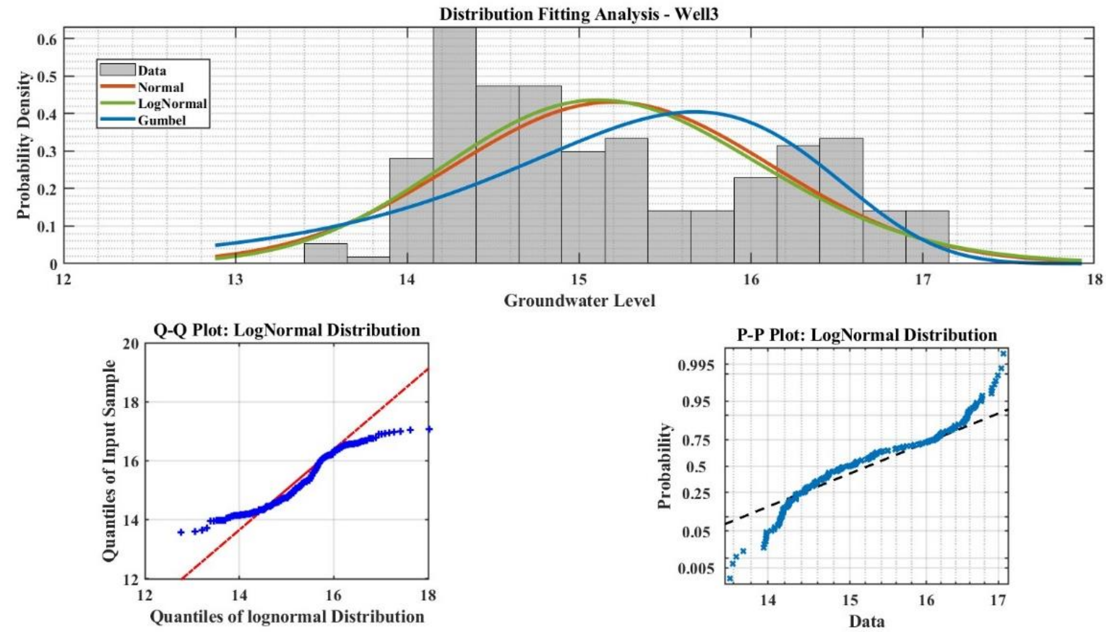

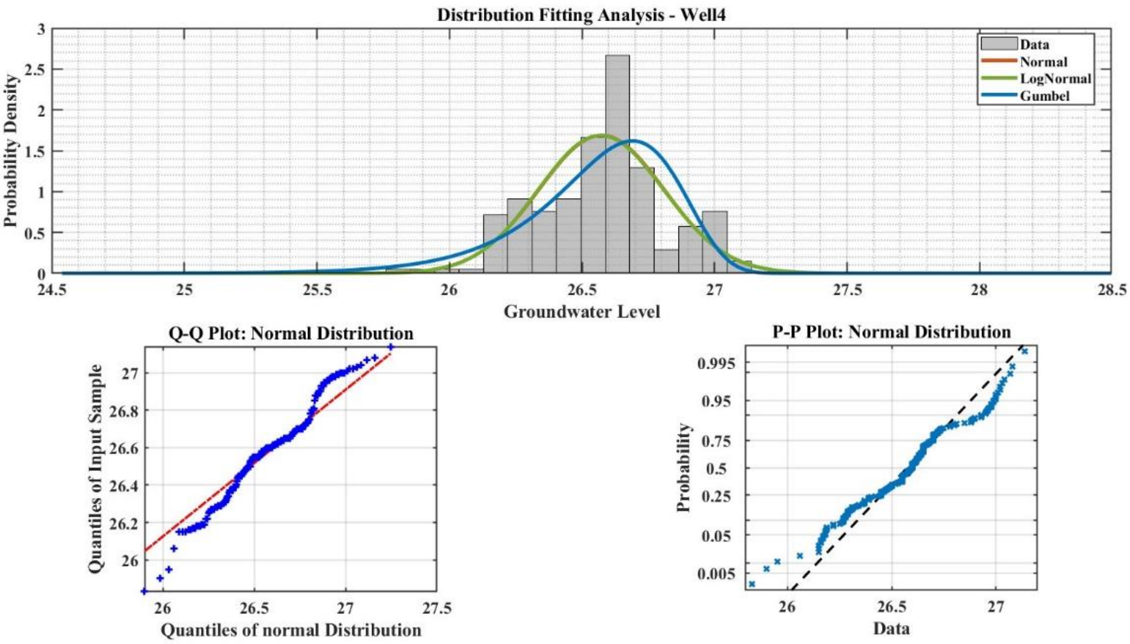

Figure 2. Continued

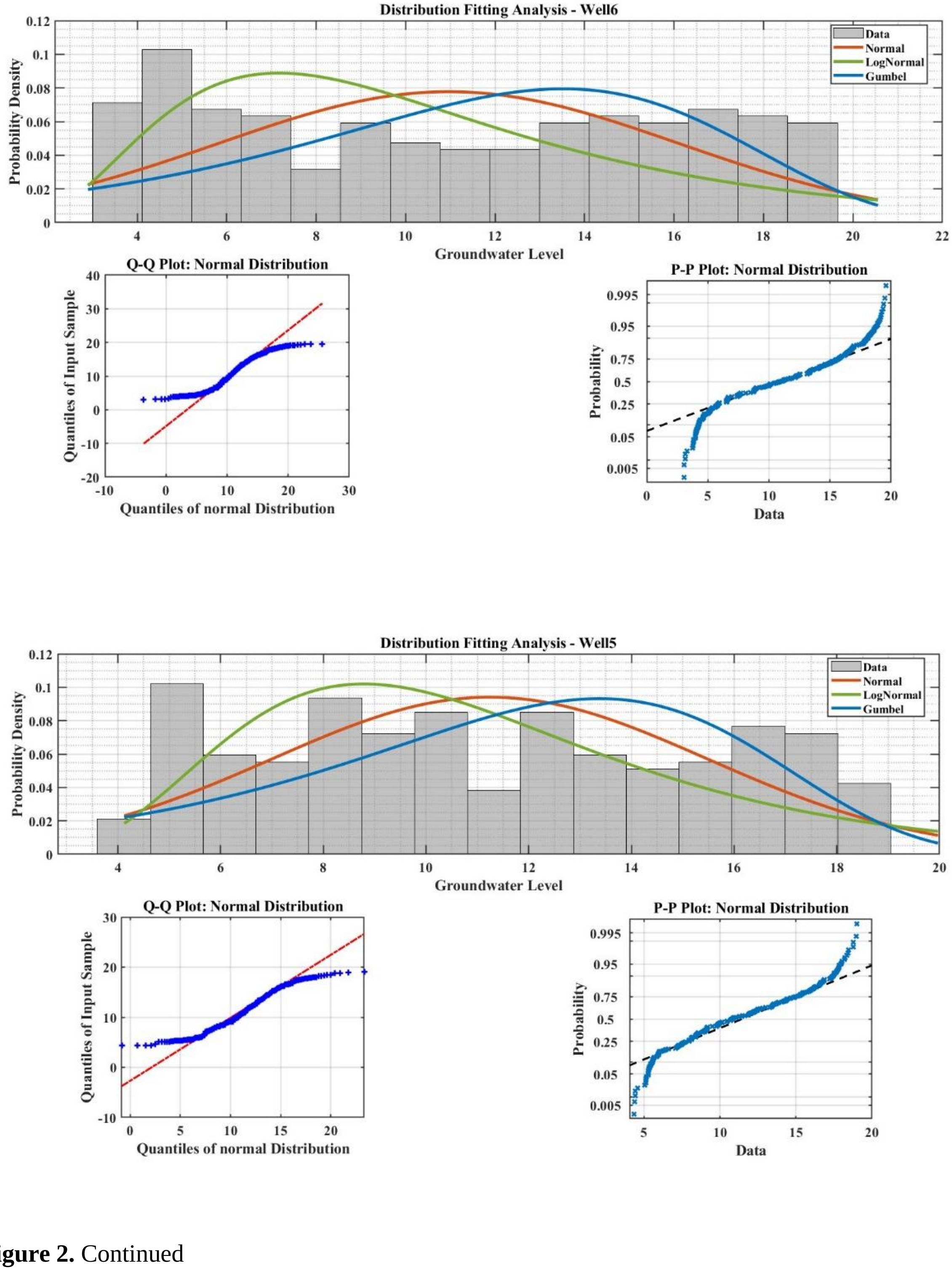

Figure 2. Continued

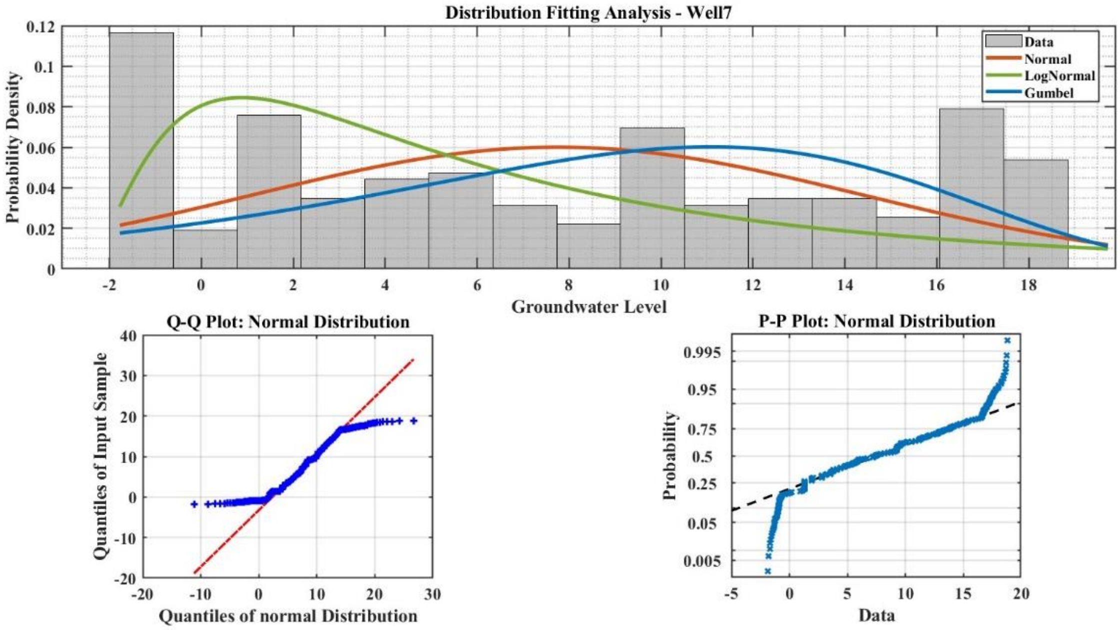

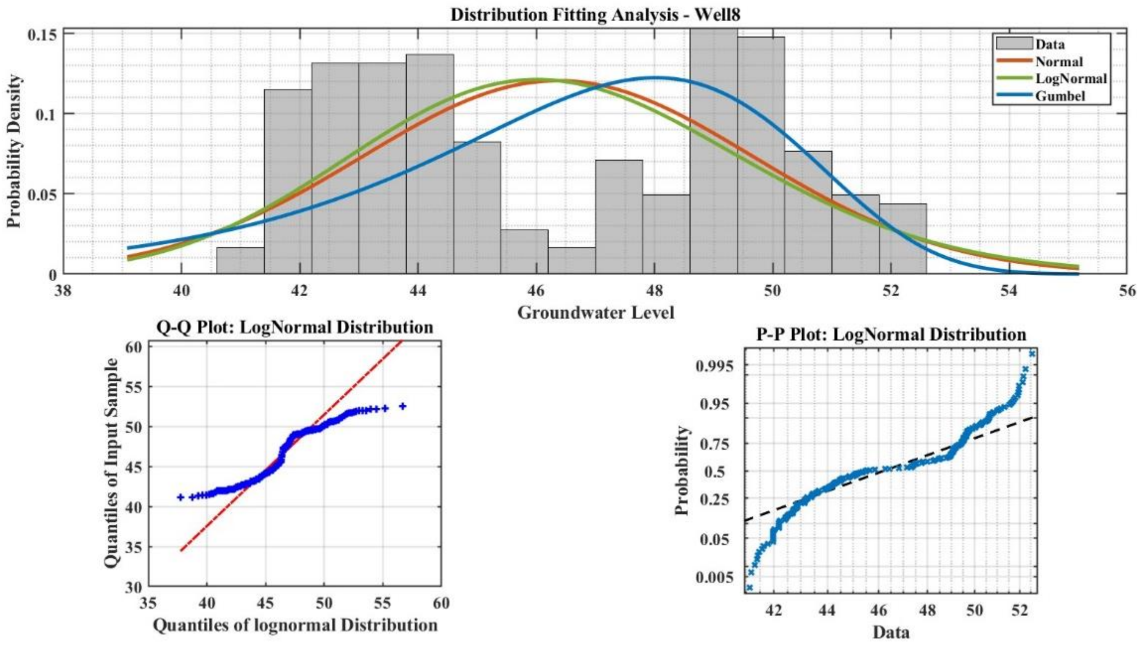

Figure 2. Continued

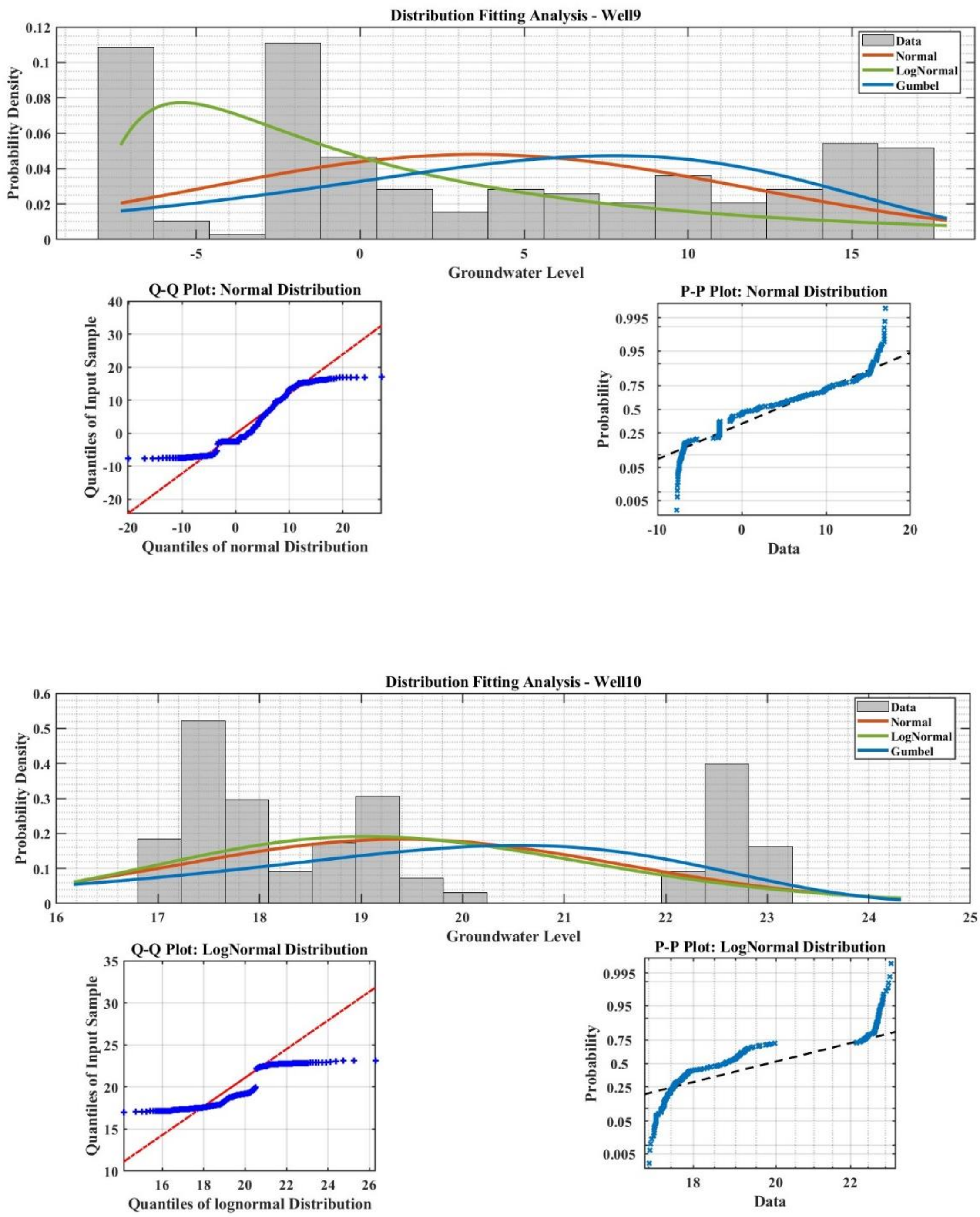

Figure 2. Continued

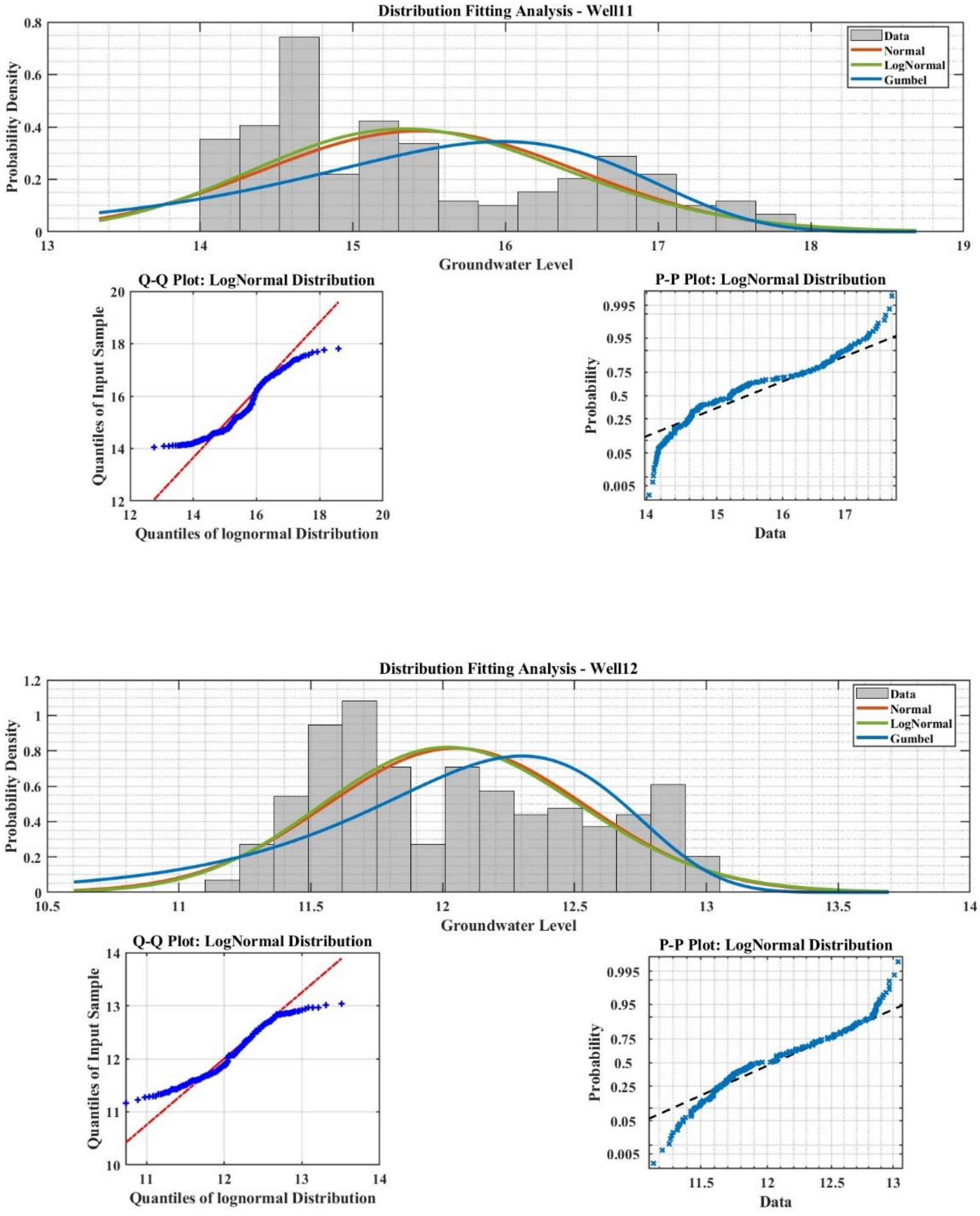

Figure 2. Continued

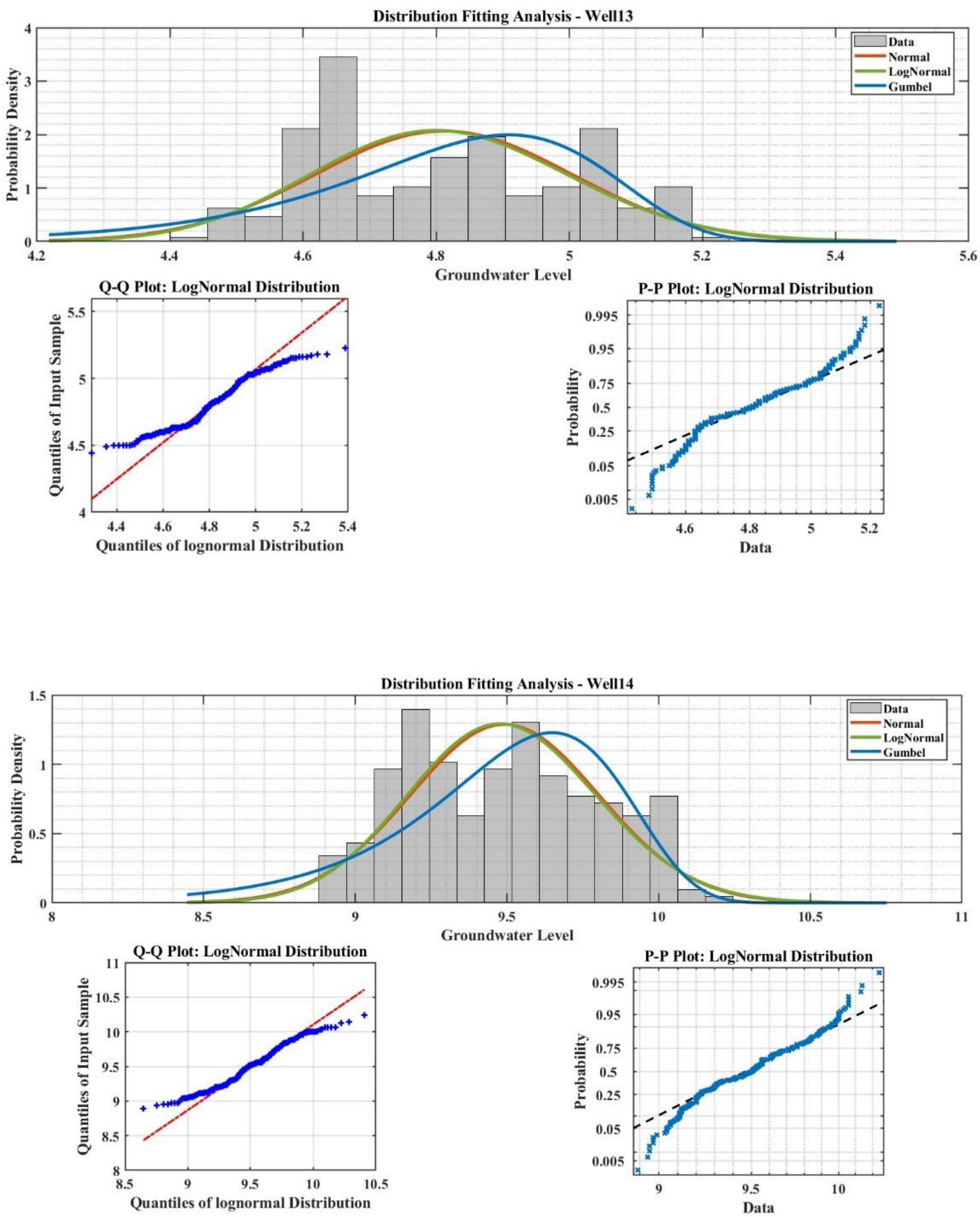

Figure 2. Continued

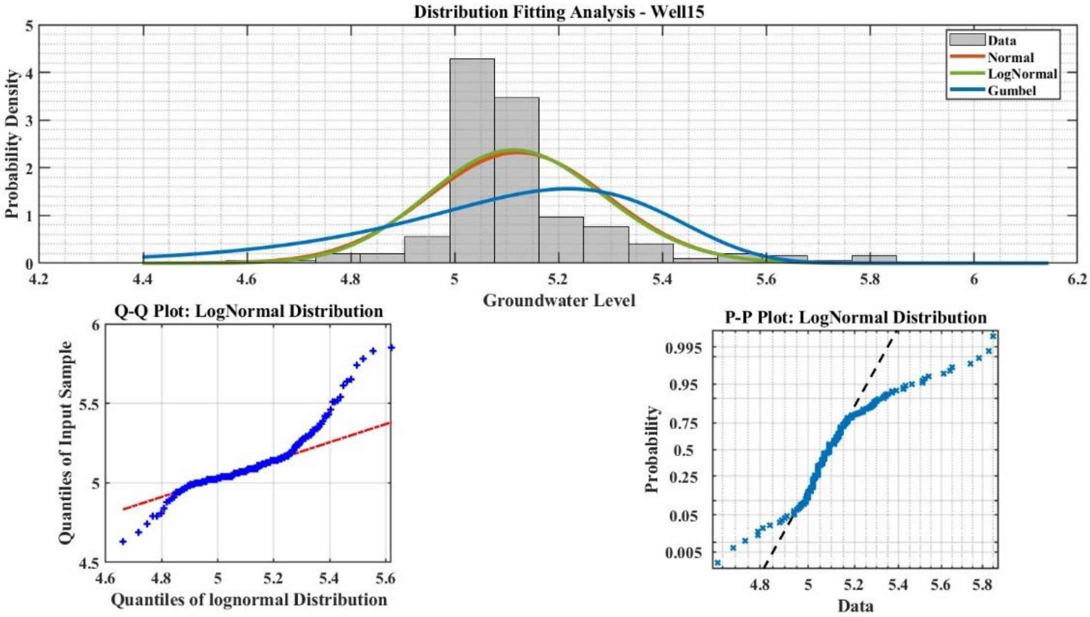

Figure 2. Continued

Table 2. Statistical Test Results and Distribution Analysis for Groundwater Wells

Well	KS_Best	KS_pValue	AD_Best	AD_pValue	Chi2_Best	Chi2_pValue	Overall_Best_Distribution	Average_pValue
Well1	Normal	0.02053	Normal	0.0005	Normal	1.54E-08	Normal	0.00701
Well2	LogNormal	0.008916	Normal	0.0005	LogNormal	7.58E-08	LogNormal	0.003139
Well3	LogNormal	0.002516	Normal	0.0005	LogNormal	4.17E-15	LogNormal	0.001005
Well4	Normal	0.027868	Normal	0.0005	Normal	1.05E-05	Normal	0.009459
Well5	LogNormal	0.040411	Normal	0.0005	Normal	0.004589	LogNormal	0.013639
Well6	Normal	0.003376	Normal	0.0005	Normal	0.000215	Normal	0.001364
Well7	Normal	0.017776	Normal	0.0005	Normal	4.32E-05	Normal	0.006106
Well8	Normal	6.50E-05	Normal	0.0005	Normal	6.51E-14	Normal	0.000188
Well9	Normal	0.000561	Normal	0.0005	LogNormal	1.13E-12	Normal	0.000354
Well10	LogNormal	6.48E-07	Normal	0.0005	LogNormal	6.09E-27	LogNormal	0.000167
Well11	LogNormal	0.000717	Normal	0.0005	LogNormal	6.00E-12	LogNormal	0.000406
Well12	LogNormal	0.006193	Normal	0.0005	LogNormal	5.48E-07	LogNormal	0.002231
Well13	LogNormal	0.001316	Normal	0.0005	LogNormal	7.64E-08	LogNormal	0.000606
Well14	LogNormal	0.092784	Normal	0.0005	LogNormal	2.53E-05	LogNormal	0.031103
Well15	LogNormal	5.89E-06	Normal	0.0005	LogNormal	1.47E-13	LogNormal	0.000169

Four representative wells (WELL1, WELL5, WELL10, and WELL15) were selected to visualize model performance (Fig. 3), though all 15 wells were used in the analysis. Fig. 3 illustrates the correlation between observed and predicted groundwater levels across three time windows using GMDH, GMDH-GA, and GMDH-HS models. Analysis of groundwater level variations reveals distinct spatial patterns. Over the study period, groundwater levels in the northwestern region, characterized by high well density and good water quality, decreased from 15-19 meters to 7-11 meters. As a result of excessive extraction and limited recharge during drought conditions, this decline has occurred. This pattern is accurately captured by all three models, with GMDH-HS exhibiting the closest fit to the observed fluctuations, particularly during peak drops. Because of its flat topography, proximity to the Persian Gulf, and consistent recharge from saline rivers, the Southeast region, represented by wells 1 and 15, maintained relatively stable levels (fluctuating only between 4.7-5.4m). These wells exhibited the highest R^2 and Willmott index values in GMDH-HS predictions, confirming the model's effectiveness in low-variability conditions. During the model performance analysis, these hydrogeological differences significantly influenced the correlation patterns between measured and predicted values.

Table 3 presents a comparative analysis of three GMDH-based models (GMDH, GMDH-GA, and GMDH-HS) across 15 observation windows (OBW1-OBW15) and three-time steps. The evaluation metrics include Efficiency Factor (EF), Coefficient of Likelihood (CL), Willmott Index (d), Root Mean Square Error (RMSE), and Coefficient of Determination (R^2). GMDH-HS consistently outperforms GMDH and GMDH-GA across most metrics, particularly in terms of EF and d.

Fig. 4 presents a comprehensive comparison of model performance across three time periods using four metrics—RMSE, Efficiency Factor (EF), Willmott Index (d), and R^2—for the GMDH, GMDH-GA, and GMDH-HS models. Several key observations emerge from this comparison. First, the GMDH-HS model consistently outperforms both GMDH and GMDH-GA across all metrics and time periods, exhibiting lower RMSE values (indicating improved prediction accuracy), higher Willmott Index values (signifying better agreement between predicted and observed values), and higher R^2 values (demonstrating stronger explanatory power). Second, model performance generally improves from the first to the third time period across all three models, suggesting enhanced predictive capability over longer temporal horizons. Collectively, these findings highlight the effectiveness of the hybrid GMDH-HS model in improving prediction accuracy, reliability, and overall performance for groundwater level forecasting in the Kahoorestan Plain.

Fig. 5 presents a comparative spatial analysis of groundwater levels (GWL) and pumping rates using three interpolation methods: Inverse Distance Weighting (IDW), Spline, and Kriging. The left panels (a-c) illustrate the spatial distribution of GWL, ranging from 4.821 to 47.202 meters. The right panels (d-f) display the spatial distribution of pumping rates, which vary from 0 to 8.30×10^6 m^3/year. IDW interpolation (a,d) exhibits more pronounced local variations and sharper transitions, particularly in the western region. Spline interpolation (b,e) produces smoother transitions while capturing the overall spatial patterns. Kriging interpolation (c,f) provides a balanced representation, effectively capturing both local variations and regional trends. A notable spatial pattern is the higher GWL in the western portion, coinciding with areas of intensive pumping (darker colors in d-f). While all three methods capture the general spatial distribution, Kriging provides the most statistically robust representation of both GWL and pumping rates. This makes it particularly suitable for hydrogeological modeling in this region. This spatial analysis offers crucial insights into the relationship between GWL and extraction rates, which are essential for sustainable aquifer management.

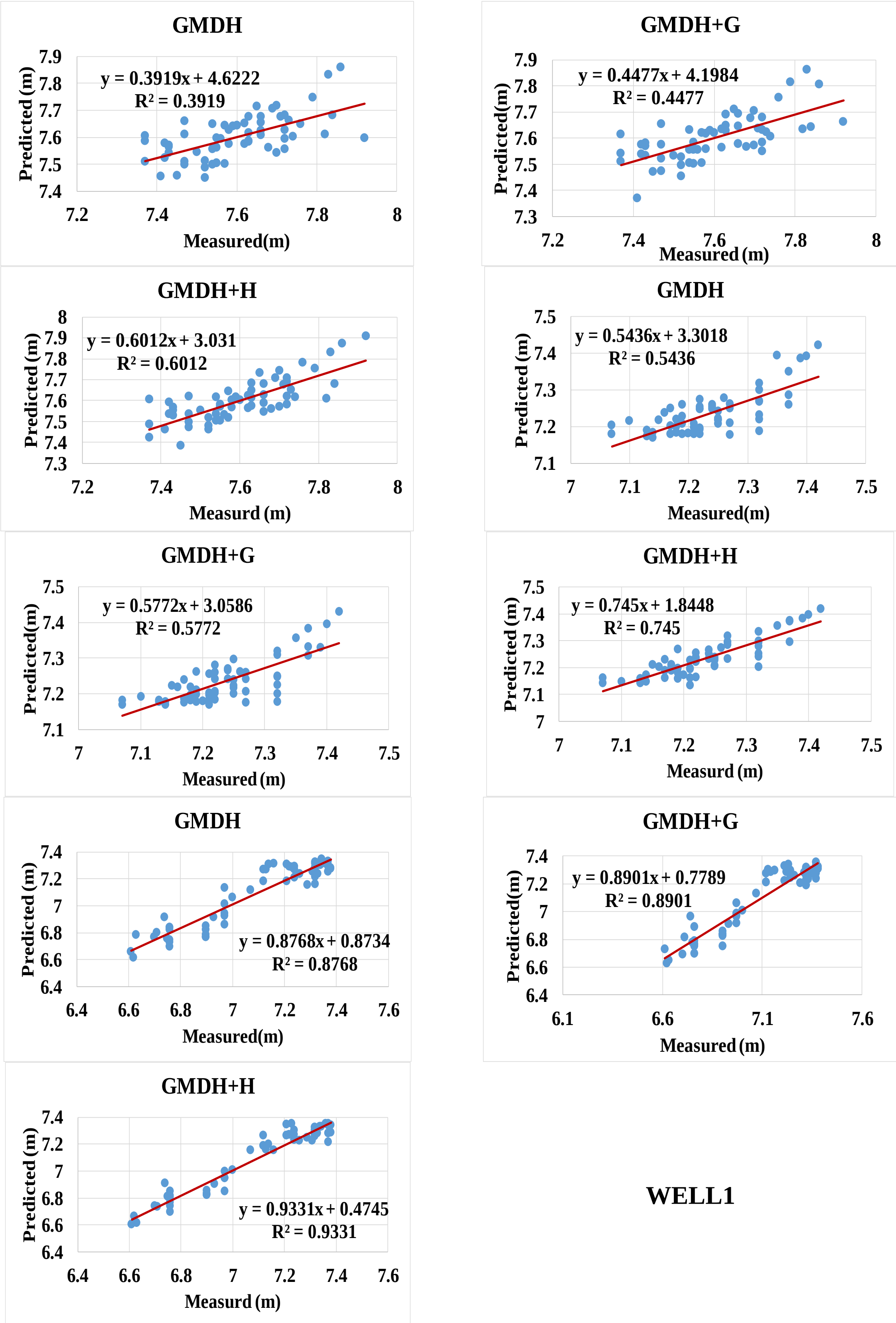

Figure 3. Correlation between Measured and Predicted Values for Three Time Periods (5 years) Using GMDH, GMDH-G, and GMDH-HS Models to WELL1, WELL5, Well10, Well15.

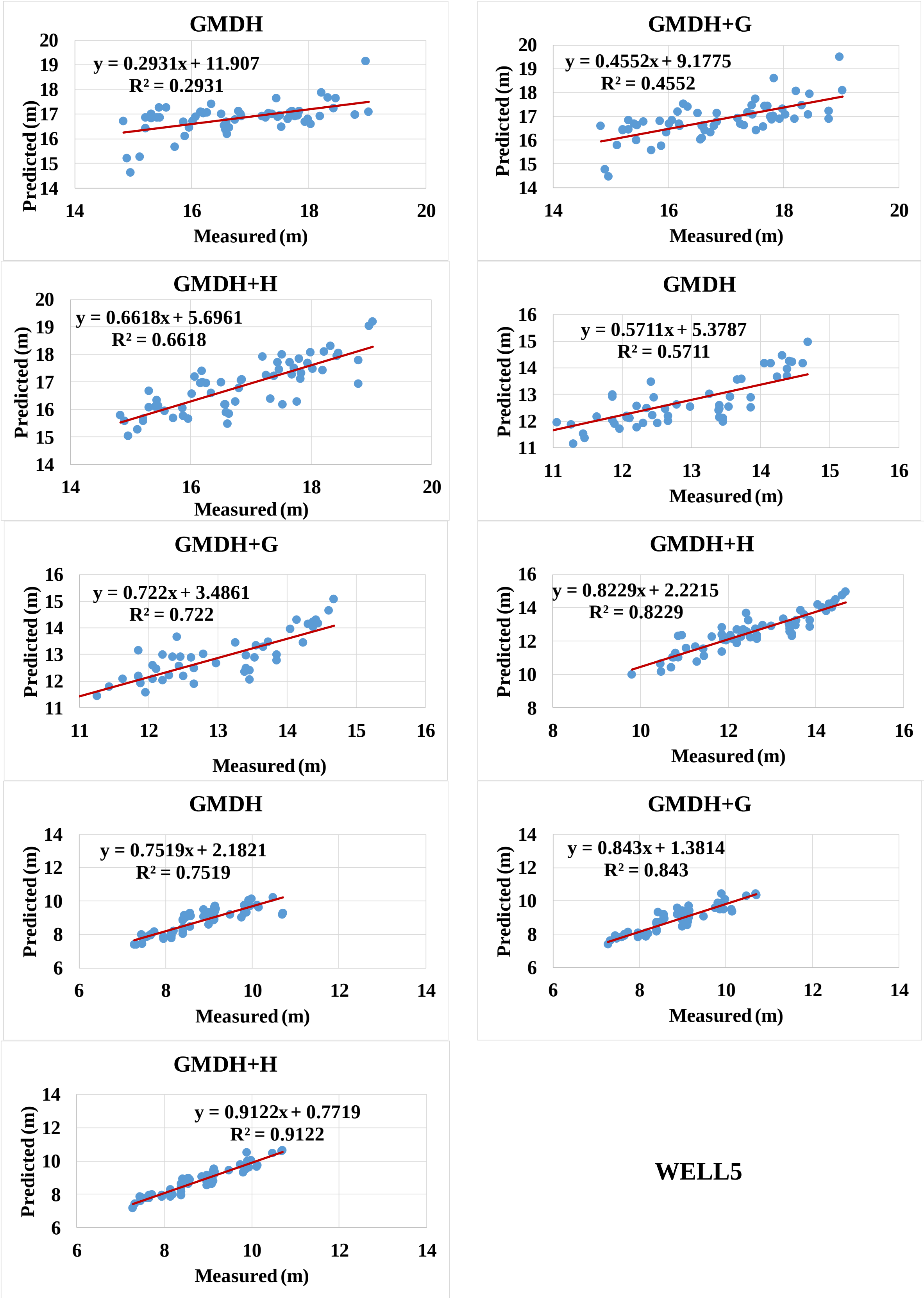

Fugure 3. Continued

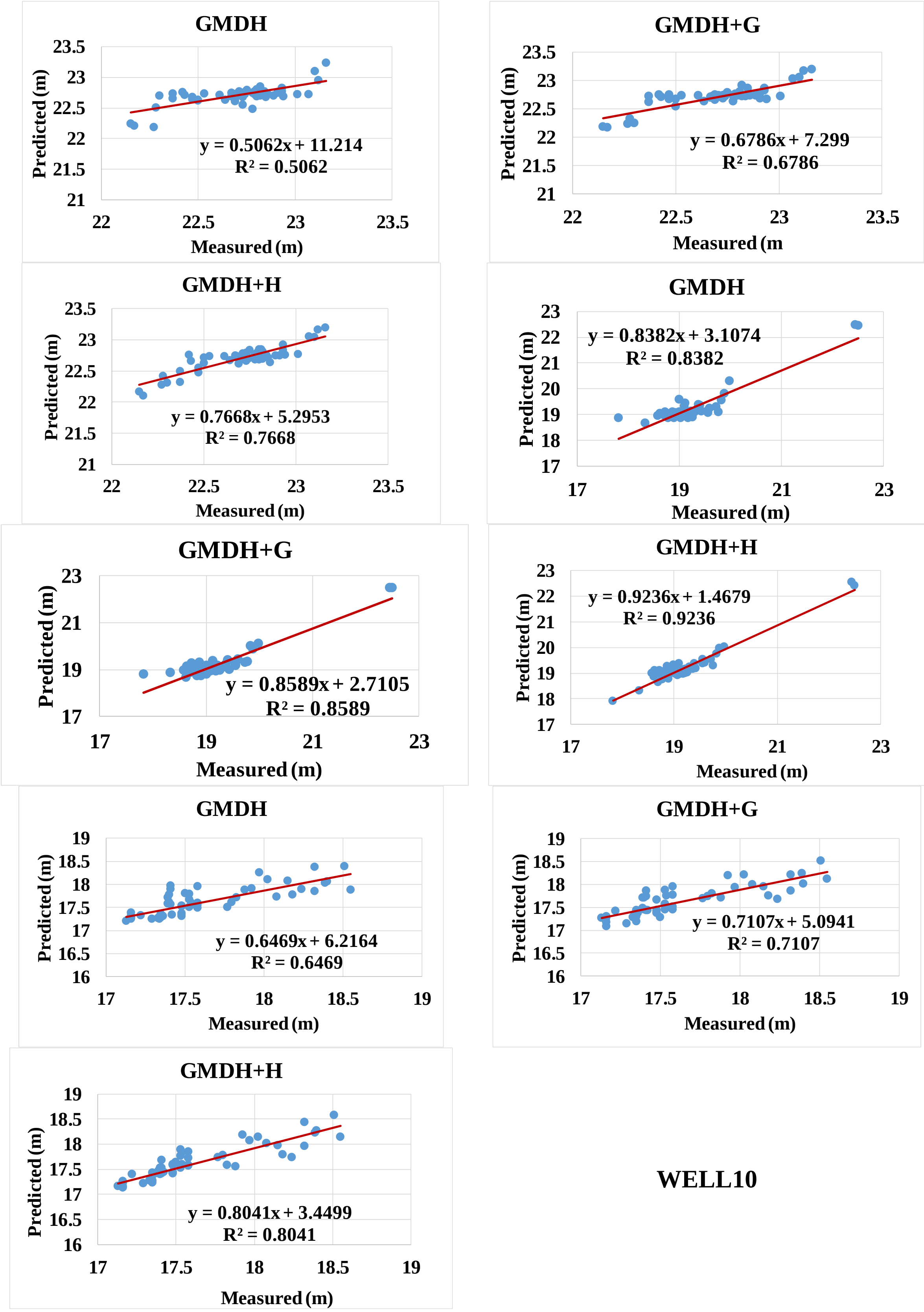

Fugure 3. Continued

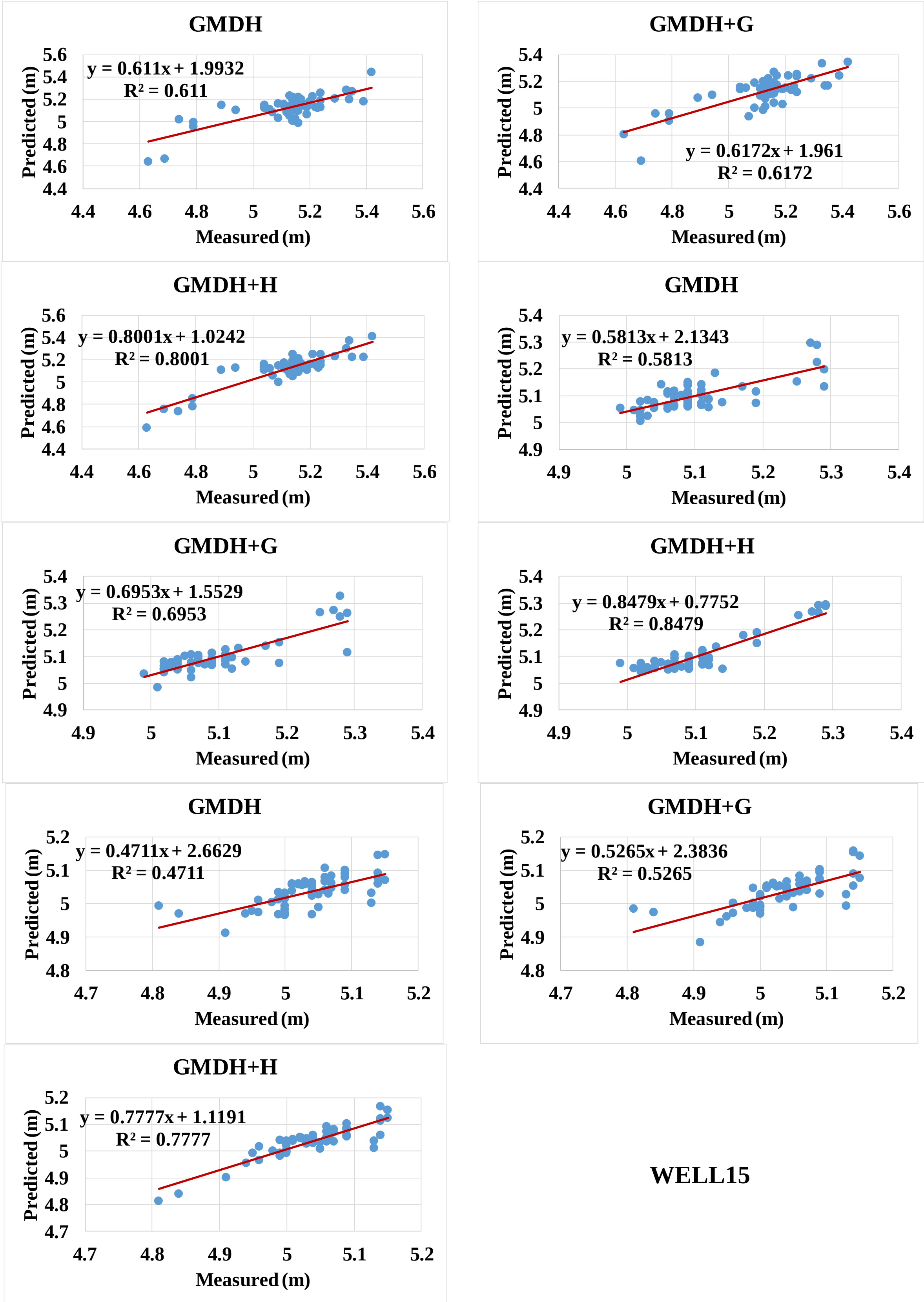

Fugure 3. Continued

Table 3. Comparative Analysis of GMDH Models Using Multiple Performance Metrics Across 15 Observation Windows

GMDH	EF5-1st	EF5-2nd	EF5-3st	CL5-1st	CL5-2nd	CL5-3st	d5-1st	d5-2nd	d5-3st	RMSE5-1st	RMSE5-2nd	RMSE5-3st	$R^2$5-1st	$R^2$5-2nd	$R^2$5-3st
OBW1	0.4020	0.5512	0.8789	0.2959	0.4605	0.8491	0.7361	0.8354	0.9661	0.1027	0.0534	0.0865	0.6323	0.7417	0.9374
OBW2	0.4084	0.6391	0.7901	0.3047	0.5611	0.7406	0.7461	0.8780	0.9374	0.0887	0.0914	0.0711	0.6373	0.7990	0.8888
OBW3	0.4317	0.6910	0.8171	0.3309	0.6228	0.7734	0.7667	0.9013	0.9465	0.2070	0.1826	0.0875	0.6555	0.8310	0.9038
OBW4	0.2720	0.3895	0.8291	0.1702	0.2828	0.7881	0.6258	0.7260	0.9505	0.1335	0.0504	0.0442	0.5178	0.6221	0.9105
OBW5	0.3049	0.5783	0.7561	0.1992	0.4921	0.6993	0.6533	0.8510	0.9249	0.9689	0.8291	0.4422	0.5490	0.7598	0.8693
OBW6	0.3453	0.6446	0.7767	0.2418	0.5682	0.7243	0.7005	0.8816	0.9325	0.9917	0.8834	0.7166	0.5851	0.8650	0.8812
OBW7	0.3384	0.6355	0.8162	0.2318	0.5579	0.7721	0.6852	0.8779	0.9460	1.2643	1.1377	0.7229	0.5791	0.7968	0.9033
OBW8	0.4074	0.5744	0.6270	0.3042	0.4865	0.5457	0.7467	0.8468	0.8703	0.9081	1.1298	0.5486	0.6365	0.7573	0.7914
OBW9	0.4248	0.5733	0.5854	0.3227	0.4866	0.5008	0.7596	0.8489	0.8555	1.3538	1.9420	0.6899	0.6502	0.7565	0.7645
OBW10	0.5144	0.8409	0.6530	0.4171	0.8027	0.5776	0.8108	0.9545	0.8846	0.1565	0.2857	0.2280	0.7163	0.9169	0.8077
OBW11	0.4388	0.6681	0.7074	0.3348	0.5956	0.6415	0.7631	0.8914	0.9068	0.2983	0.2007	0.1478	0.6609	0.8170	0.8408
OBW12	0.4204	0.4971	0.7494	0.3160	0.4000	0.6922	0.7515	0.8047	0.9236	0.1422	0.1281	0.0737	0.6468	0.7040	0.8655
OBW13	0.6348	0.6391	0.4966	0.5550	0.5608	0.3999	0.8743	0.8775	0.8053	0.0430	0.0407	0.0364	0.7990	0.7963	0.7037
OBW14	0.4980	0.5854	0.6584	0.4009	0.5001	0.5832	0.8050	0.8544	0.8858	0.0987	0.0643	0.0525	0.7046	0.7645	0.8110
OBW15	0.6174	0.5882	0.4799	0.5349	0.5027	0.3795	0.8663	0.8547	0.7908	0.0936	0.0468	0.0484	0.7853	0.7664	0.6916

Table 3. Continued

GMDH+GA	EF5-1st	EF5-2nd	EF5-3st	CL5-1st	CL5-2nd	CL5-3st	d5-1st	d5-2nd	d5-3st	RMSE5-1st	RMSE5-2nd	RMSE5-3st	$R^2$5-1st	$R^2$5-2nd	$R^2$5-3st
OBW1	0.4569	0.5843	0.8920	0.3543	0.4992	0.8653	0.7755	0.8543	0.9701	0.0979	0.0514	0.0816	0.6746	0.7638	0.9444
OBW2	0.4703	0.7072	0.8253	0.3725	0.6414	0.7836	0.7921	0.9070	0.9495	0.0839	0.0824	0.0649	0.6845	0.8407	0.9084
OBW3	0.5890	0.7095	0.8260	0.5028	0.6443	0.7843	0.8537	0.9081	0.9496	0.1760	0.1771	0.0854	0.7669	0.8421	0.9088
OBW4	0.4319	0.4672	0.8443	0.3310	0.3635	0.8066	0.7663	0.7781	0.9553	0.1180	0.0471	0.0422	0.6556	0.6823	0.9188
OBW5	0.4642	0.7267	0.8456	0.3611	0.6644	0.8084	0.7778	0.9144	0.9560	0.8506	0.6675	0.3519	0.6801	0.8522	0.9195
OBW6	0.3776	0.6832	0.7853	0.2707	0.6125	0.7346	0.7168	0.8966	0.9354	0.9669	0.8340	0.7026	0.6124	0.8534	0.8861
OBW7	0.4070	0.7513	0.8402	0.3002	0.6940	0.8015	0.7376	0.9237	0.9539	1.1969	0.9398	0.6741	0.6362	0.8666	0.9166
OBW8	0.5528	0.5911	0.6945	0.4619	0.5056	0.6260	0.8357	0.8553	0.9013	0.7889	1.1075	0.4965	0.7427	0.7682	0.8331
OBW9	0.4565	0.7094	0.6729	0.3524	0.6432	0.6010	0.7719	0.9067	0.8932	1.3160	1.6027	0.6127	0.6743	0.8420	0.8200
OBW10	0.6839	0.8612	0.7157	0.6131	0.8275	0.6512	0.8965	0.9608	0.9100	0.1262	0.2668	0.2064	0.8267	0.9280	0.8457
OBW11	0.4783	0.7868	0.7493	0.3779	0.7368	0.6914	0.7902	0.9364	0.9228	0.2876	0.1609	0.1368	0.6904	0.8869	0.8654
OBW12	0.5953	0.5734	0.8232	0.5106	0.4862	0.7811	0.8577	0.8479	0.9489	0.1189	0.1180	0.0619	0.7710	0.7566	0.9072
OBW13	0.6991	0.6829	0.6262	0.6314	0.6126	0.5463	0.9032	0.8970	0.8723	0.0390	0.0381	0.0314	0.8261	0.8358	0.7909
OBW14	0.6587	0.6039	0.7427	0.5827	0.5197	0.6837	0.8847	0.8606	0.9206	0.0814	0.0629	0.0456	0.8112	0.7766	0.8616
OBW15	0.6236	0.7004	0.5344	0.5419	0.6328	0.4411	0.8690	0.9035	0.8253	0.0928	0.0400	0.0458	0.7892	0.8366	0.7302

Table 3. Continued

GMDH+H	EF5-1st	EF5-2nd	EF5-3st	CL5-1st	CL5-2nd	CL5-3st	d5-1st	d5-2nd	d5-3st	RMSE5-1st	RMSE5-2nd	RMSE5-3st	$R^2$5-1st	$R^2$5-2nd	$R^2$5-3st
OBW1	0.6079	0.7493	0.9342	0.5237	0.6913	0.9177	0.8616	0.9227	0.9824	0.0832	0.0399	0.0637	0.7791	0.8654	0.9665
OBW2	0.6192	0.8063	0.8959	0.5365	0.7605	0.8702	0.8665	0.9432	0.9714	0.0712	0.0670	0.0501	0.7864	0.8978	0.9465
OBW3	0.6972	0.8138	0.8930	0.6287	0.7696	0.8667	0.9017	0.9457	0.9706	0.1511	0.1418	0.0669	0.8347	0.9020	0.9449
OBW4	0.5417	0.6250	0.8923	0.4472	0.5434	0.8657	0.8255	0.8694	0.9702	0.1060	0.0395	0.0351	0.7352	0.7901	0.9446
OBW5	0.6675	0.8258	0.9137	0.5945	0.7841	0.8924	0.8906	0.9495	0.9767	0.6701	0.5328	0.2630	0.8166	0.9087	0.9559
OBW6	0.5942	0.7951	0.8532	0.5083	0.7466	0.8176	0.8555	0.9390	0.9583	0.7808	0.6707	0.5810	0.7703	0.8959	0.9236
OBW7	0.6482	0.8216	0.9114	0.5702	0.7788	0.8894	0.8797	0.9478	0.9759	0.9219	0.7960	0.5020	0.8047	0.9063	0.9546
OBW8	0.6986	0.7528	0.7654	0.6304	0.6959	0.7108	0.9025	0.9244	0.9287	0.6477	0.8610	0.4351	0.8355	0.8675	0.8747
OBW9	0.7019	0.7457	0.8201	0.6348	0.6868	0.7772	0.9044	0.9209	0.9477	0.9746	1.4991	0.4544	0.8375	0.8634	0.9055
OBW10	0.7707	0.9248	0.8074	0.7173	0.9062	0.7617	0.9307	0.9798	0.9433	0.1075	0.1964	0.1698	0.8777	0.9617	0.8985
OBW11	0.6696	0.9005	0.8490	0.5963	0.8760	0.8126	0.8904	0.9728	0.9572	0.2289	0.1099	0.1062	0.8180	0.9489	0.9213
OBW12	0.7076	0.7274	0.9015	0.6409	0.6648	0.8773	0.9057	0.9140	0.9731	0.1010	0.0943	0.0462	0.8410	0.8527	0.9494
OBW13	0.8278	0.7642	0.7457	0.7866	0.7093	0.6868	0.9502	0.9281	0.9211	0.0295	0.0329	0.0259	0.8740	0.9098	0.8633
OBW14	0.7854	0.7439	0.8421	0.7351	0.6851	0.8042	0.9359	0.9209	0.9550	0.0645	0.0506	0.0357	0.8861	0.8623	0.9176
OBW15	0.8034	0.8505	0.7814	0.7566	0.8144	0.7304	0.9418	0.9577	0.9347	0.0671	0.0282	0.0314	0.8962	0.9221	0.8838

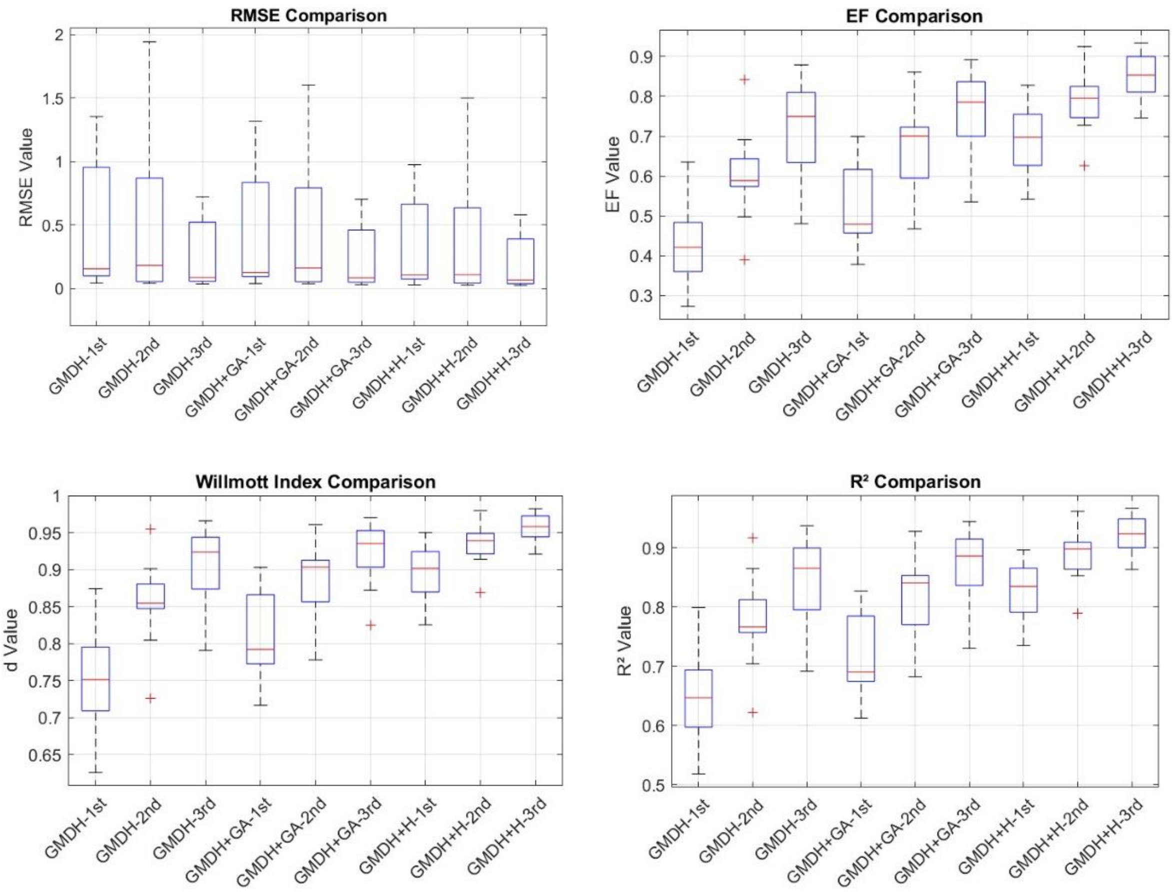

Figure 4. Statistical Performance Analysis of GMDH-Based Models for Groundwater Level Prediction

Fig. 6 illustrates the temporal evolution of groundwater levels (GWL) across three time periods: current (t), 5-year projection (t+5), and 10-year projection (t+10) using the GMDH-HS model. At the current time (t), GWL ranges from 5.051 to 50.127 meters, with higher levels concentrated in the western region. The 5-year projection (t+5) indicates a moderate decline in maximum GWL to 48.191 meters, while minimum levels remain relatively stable at 4.801 meters. This suggests a gradual depletion of groundwater resources. The 10-year projection (t+10) shows a more significant decline, with the maximum GWL decreasing to 43.287 meters and the minimum levels dropping below the surface level to -1.851 meters, particularly evident in the eastern portions. These projected declines align with observed over-extraction trends and limited recharge in the region, validating the model's responsiveness to physical stress conditions. This temporal analysis reveals a concerning trend of groundwater depletion, with the western region maintaining relatively higher levels while the eastern sector shows increased vulnerability to groundwater stress. The emergence of negative GWL values indicates severe aquifer stress that could lead to dry wells or saltwater intrusion. The progressive reduction in GWL values, especially the emergence of negative values in the 10-year projection, suggests significant aquifer stress and potential overexploitation. This highlights the urgent need for sustainable groundwater management strategies in the region.

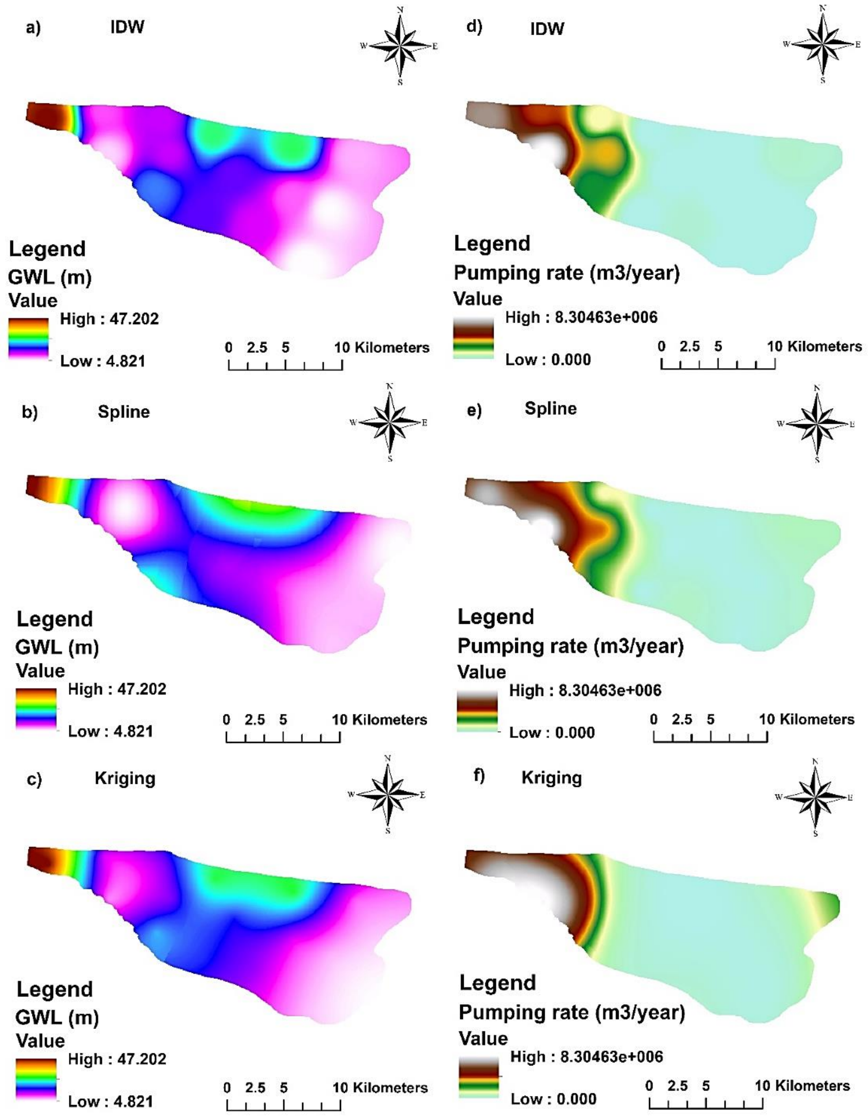

Figure 5. Spatial Analysis of Groundwater Characteristics Using Three Interpolation Techniques

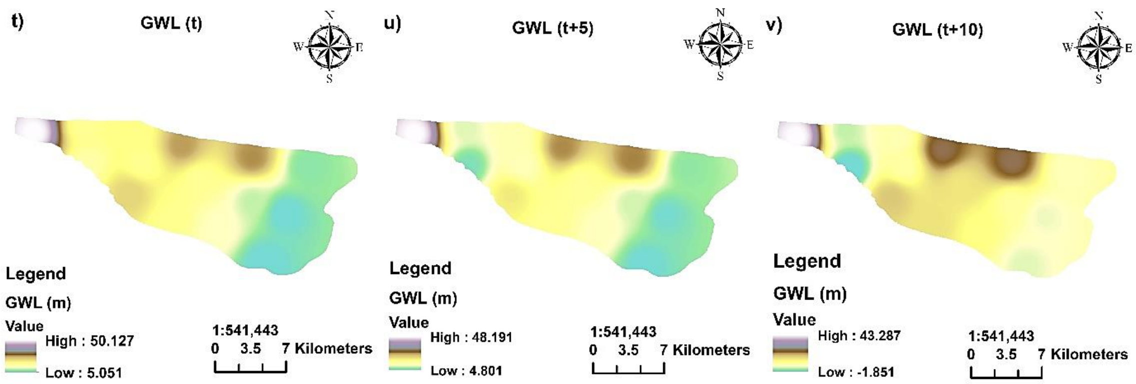

Figure 6. Spatial-Temporal Prediction of Groundwater Levels for Current and Future Time Windows

Fig. 7 illustrates the spatial distribution of RMSE for standard GMDH, GMDH-GA, and GMDH-HS models across multiple time horizons (current, t+5, and t+10). Over the 15-year study period, GMDH-HS exhibited superior performance with the lowest RMSE ranges across all temporal scenarios: 0.054–2.705 (15-year), 0.029–0.974 (current), 0.028–1.499 (t+5), and 0.025–0.680 (t+10), consistently outperforming GMDH-GA (0.058–2.768, 0.038–1.316, 0.038–1.602, and 0.031–0.702, respectively) and standard GMDH (0.063–2.597, 0.042–1.353, 0.040–1.942, and 0.036–0.722, respectively). Spatially, lower RMSE values in the western region reflect relatively stable groundwater recharge from upstream inflows, while higher errors in the eastern region indicate prediction challenges due to saltwater intrusion, intensive agricultural extraction, and low recharge rates. The progressive reduction in RMSE from GMDH to GMDH-GA to GMDH-HS—consistent across all temporal scales—validates the effectiveness of the hybrid approach. The decreasing RMSE in 10-year projections demonstrates GMDH-HS's ability to capture long-term trends, making it suitable for strategic planning and early warning systems. High-error regions identified by the model can serve as priority zones for detailed field monitoring and adaptive management. Future refinements could incorporate additional high-resolution datasets (e.g., in-situ piezometric measurements and geological heterogeneity) to further address localized prediction errors.

The heat map in Fig. 8 compares five performance metrics (EF, CL, d, RMSE, and R^2) across three models (GMDH, GMDH-GA, and GMDH-HS) over three time periods. GMDH-HS consistently outperforms both GMDH and GMDH-GA across all metrics and periods, exhibiting the lowest RMSE values (most accurate predictions), the highest Willmott Index (d) values (best agreement between predicted and observed values), and the highest R^2 values (strongest correlation). All models show improved performance from the first to the third period, with GMDH-HS demonstrating the most significant gains.

Analysis of Uncertainty and Sensitivity of Parameters

An exhaustive uncertainty analysis was conducted to assess the robustness of predictions, including key sensitivity parameters. Random error simulations (n=1000) were performed by introducing random perturbations (±10%) to the satellite input data. GMDH-HS was the more stable predictor, with a coefficient of variation of 0.14. At the same time, GMDH-GA has a coefficient of variation of 0.23, and standard GMDH has a coefficient of variation of 0.31. This highlights the superior robustness of the GMDH-HS model in the presence of input variability, making it more suitable for real-world groundwater prediction under uncertain conditions.

The gravity data from GRACE-JPL was the most sensitive input (sensitivity index: 0.42) followed by soil moisture (0.35), precipitation (0.29), temperature (0.18), and potential evapotranspiration (0.12). These findings highlight the significant influence of GRACE data on groundwater level predictions and underscore the importance of incorporating large-scale terrestrial water storage signals into hydrological modeling.

Within GMDH-HS, harmony memory size (HMS) and harmony memory consideration rate (HMCR) were the most sensitive parameters, with HMS set to 30 and HMCR set to 0.85 being optimal for the Kahoorestan Plain. Tuning these parameters significantly enhanced model convergence and reduced prediction variance. This level of sensitivity analysis helps to refine model accuracy across different hydrogeological regions. Uncertainty arises from (1) the spatial resolution of satellite data in areas of more severe topographic complexity, (2) gaps in remote sensing observations, and (3) the oversimplification of hydrogeology. Acknowledging these sources of uncertainty enables more transparent model interpretation and provides direction for future model enhancements. Future research should focus on integrating higher-resolution satellite data and incorporating physical constraints to reduce these uncertainties.

Error distribution analysis across three-time windows reveals the superior performance of the GMDH-HS model compared to traditional GMDH and GMDH-GA variants (Fig. 9).

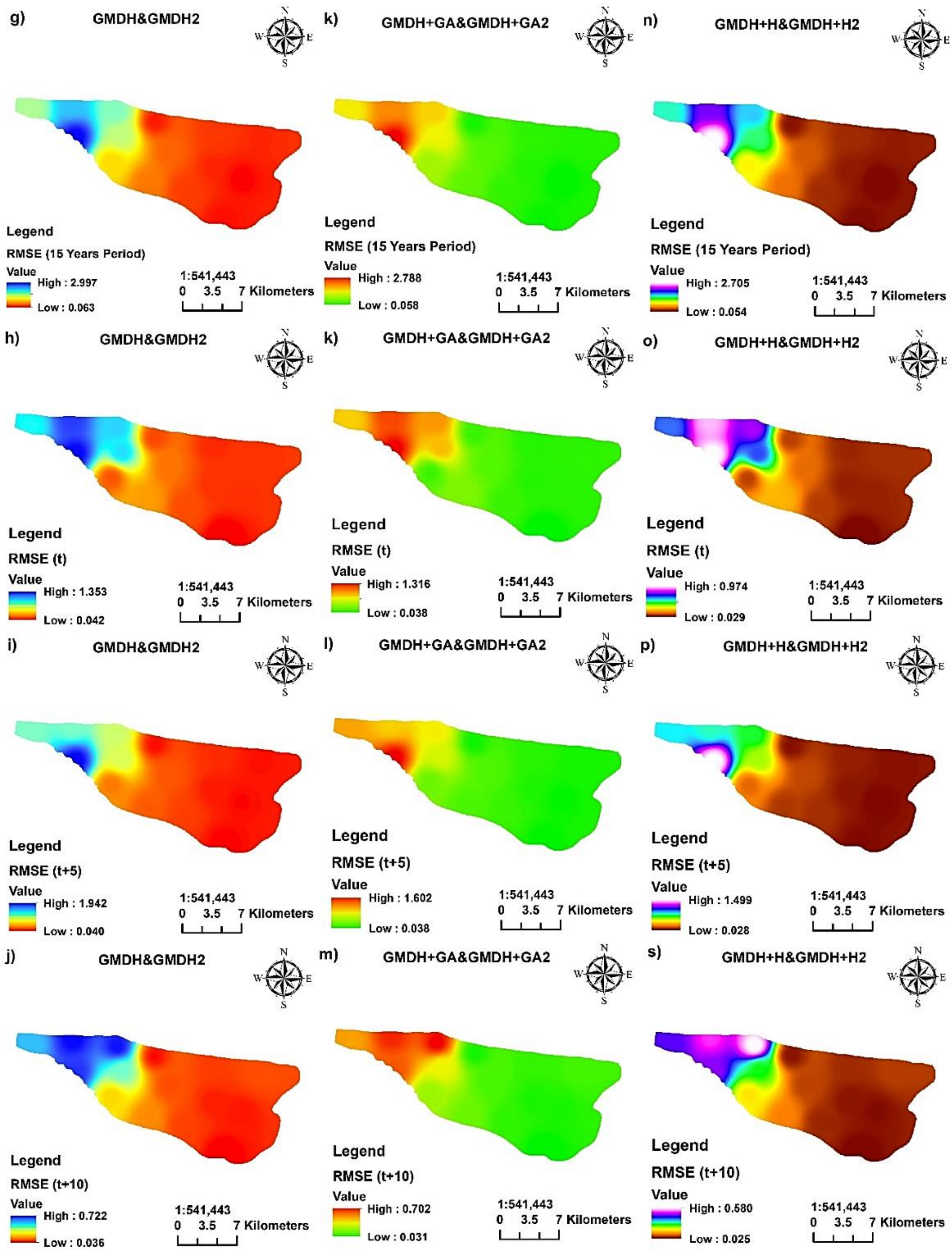

Figure 7. Comparative Spatial Analysis of RMSE for Different GMDH Model Variants and Time Periods

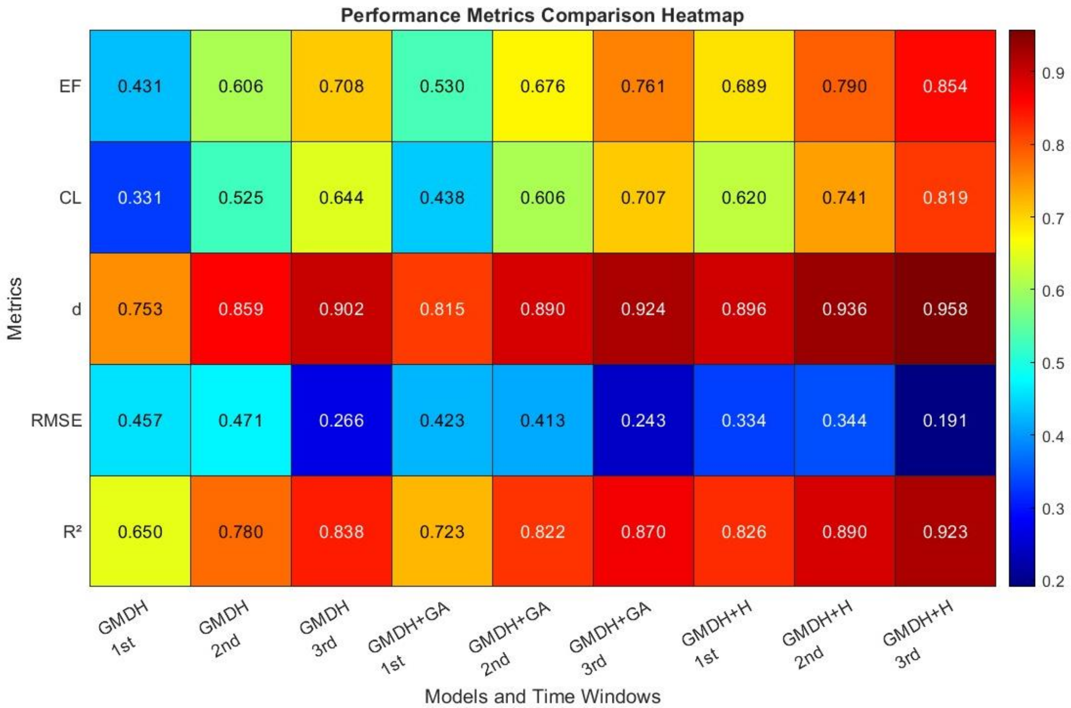

Figure 8. Performance Metrics heat map Analysis of GMDH-Based Models for Groundwater Level Prediction across Multiple Periods.

Comparatively to other models, GMDH-HS achieved consistent error reduction across all time windows. Compared to the basic GMDH, a 27% reduction in the mean error has been achieved for the first time window. Second-time window: 28% reduction over GMDH-GA. The third time window exhibits the greatest improvement, with a 39% reduction compared to the basic GMDH value. The violin plots show a narrower and more symmetrical error distribution for GMDH-HS, indicating better model stability and fewer extreme prediction errors. An analysis of the spatial distribution of prediction errors revealed that the western region had lower prediction errors than the eastern region.

The significant reduction in mean error underscores the model's ability to capture complex groundwater dynamics more accurately, resulting in more precise resource allocation and earlier detection of critical depletion zones. The consistent performance of the GMDH-HS model across all time windows indicates its robustness in capturing both short-term fluctuations and long-term trends in groundwater levels. In addition to lower mean errors, the GMDH-HS model exhibited the lowest standard deviation in each time window, signifying more uniform predictions with fewer outliers. This improved consistency is especially valuable in areas prone to significant seasonal variability.

The violin plots effectively illustrate the density and spread of errors, reinforcing the quantitative findings. The narrow and symmetric shape of the GMDH-HS distribution reflects the model’s capability to minimize large prediction errors, in contrast to the wider error distributions observed in the GMDH and GMDH-GA models. This indicates improved prediction accuracy and stability over time, making GMDH-HS a reliable tool for long-term groundwater level predictions in complex hydrogeological settings.

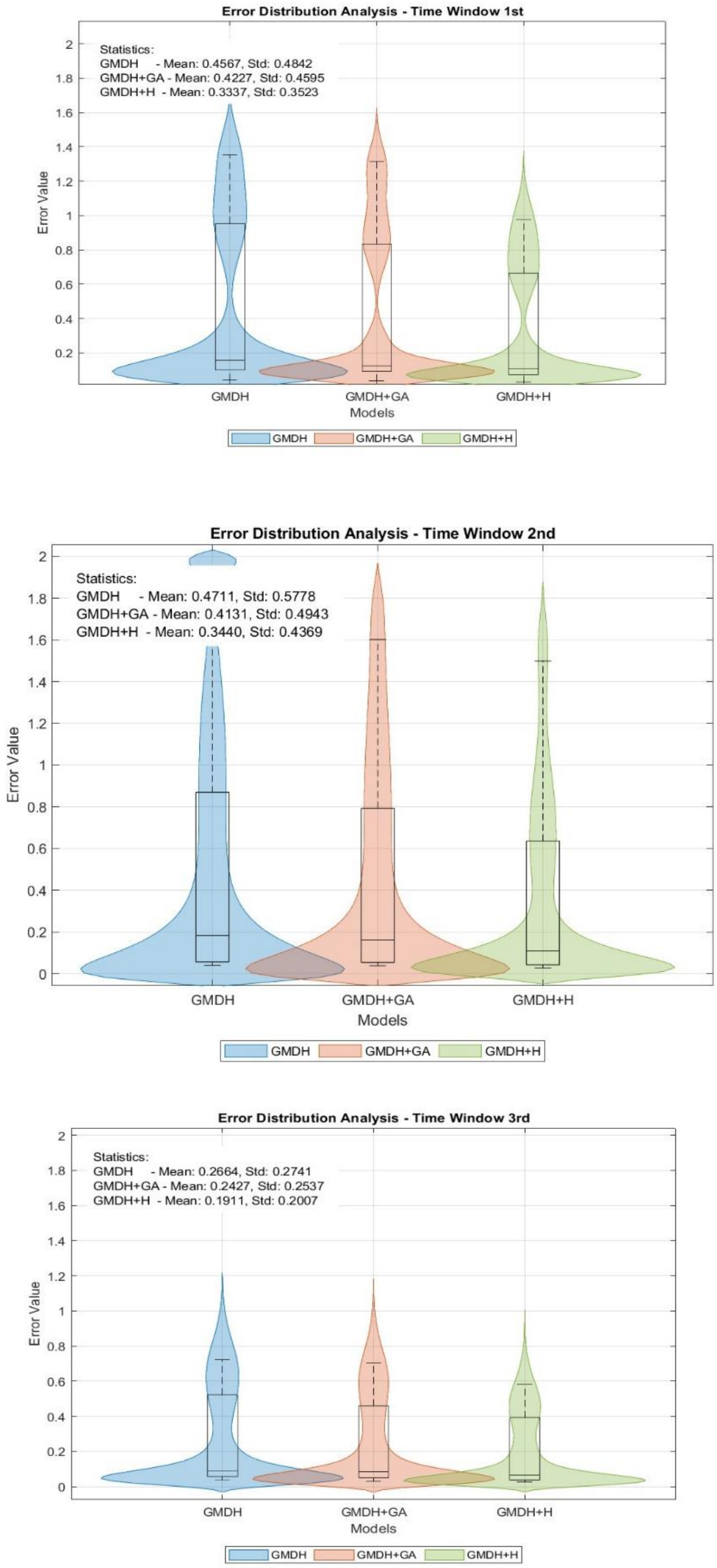

Figure 9. Error Distribution Analysis of GMDH, GMDH-GA, and GMDH-HS Models Using Violin Plots Across Three Time Windows in Groundwater Level Prediction

The GMDH-HS model demonstrated several significant advantages in comparison to the traditional GMDH and GMDH-GA models: Consistently reduced mean error by 27-39% across all time windows. High prediction reliability from the current period ($R^2 = 0.89$) to 10-year projections ($R^2 = 0.85$). Produced lower RMSE values across all 15 observation wells, particularly in hydrogeological complex areas. Compared to GMDH-GA, the algorithm achieved 40% faster convergence while maintaining a higher level of accuracy during prediction. Capability to capture complex groundwater dynamics and seasonal variations in a non-linear manner. Resulted in narrower error distributions and fewer outliers, suggesting more reliable predictions.

As a result of these advantages, GMDH-HS is well suited for groundwater level prediction in arid regions with limited data sets, where traditional modeling approaches often struggle to capture complex hydrogeological processes.

4. Discussion

The results of this study demonstrate that the GMDH-HS hybrid model significantly outperforms both standard GMDH and GMDH-GA across all evaluation metrics, achieving a 27–39% reduction in mean prediction error and R^2 values between 0.82 and 0.94. These findings are consistent with previous research highlighting the effectiveness of hybrid machine learning approaches in hydrological modeling (Tao *et al.*, 2022; Saha and Pal, 2024). The superior performance of GMDH-HS can be attributed to the Harmony Search algorithm's ability to balance global exploration and local exploitation during parameter optimization, avoiding local minima more effectively than Genetic Algorithms (Sabangban *et al.*, 2023). This aligns with observations by Dodangeh *et al.* (2020), who reported that hybrid GMDH models with metaheuristic optimization outperform standalone versions in flood susceptibility prediction. Furthermore, the 40% faster convergence achieved by GMDH-HS compared to GMDH-GA makes it particularly suitable for real-time monitoring applications in data-scarce arid regions, where computational efficiency is critical (Bamal *et al*., 2024; Shams and Muhammad, 2023).

The integration of multi-source satellite data—particularly GRACE-JPL gravity data, which exhibited the highest sensitivity index (0.42)—proved essential for capturing large-scale terrestrial water storage variations. This finding corroborates Ibrahim *et al*. (2024) and Adams *et al*. (2022), who emphasized the transformative role of GRACE and GRACE-FO missions in regional groundwater storage assessment. The observed 12% reduction in prediction errors in areas with higher-resolution data (0.25°, e.g., soil moisture and TRMM) highlights the importance of spatial resolution in satellite-based hydrological modeling (Dube *et al*., 2023; Kumar and Choudhury, 2024). However, as noted by Springer *et al*. (2023), challenges remain in integrating multi-resolution datasets, particularly in topographically complex regions. The preprocessing framework developed in this study—temporal aggregation, spatial downscaling, outlier removal, and missing data imputation—successfully mitigated these issues, providing a replicable methodology for other arid regions with sparse ground monitoring networks (Sadeghi-Lari *et al*., 2024; Scanlon *et al*., 2023).

The 10-year projections revealing a predicted groundwater level drop to -1.851 meters below surface level in the eastern Kahoorestan Plain indicate severe aquifer stress, consistent with regional observations of over-extraction and limited recharge in arid climates (El Kenawy, 2024; Rahmani *et al*., 2023). The spatial pattern of depletion—higher vulnerability in the east versus relative resilience in the northwest—reflects the combined effects of saltwater intrusion from three directions, intensive agricultural pumping, and low natural recharge rates (Safa *et al*., 2020). The dominance of Lognormal distributions in 60% of observation wells suggests positive skewness in groundwater level variations, likely due to high variability in recharge and extraction rates (Sengupta *et al*., 2022). The poor fit observed in wells 8, 10, and 15 across all distribution models highlights local hydrogeological complexities, including proximity to saline intrusion zones and structural heterogeneities, underscoring the need for site-specific analysis rather than uniform management approaches (Uddin *et al*., 2024; Sajib *et al*., 2025).

Based on GMDH-HS predictions, several management strategies are proposed for the Kahoorestan Plain. In the eastern region, where groundwater is projected to drop below surface (-1.851 m), extraction should be halted, while sustainable extraction may continue in the more resilient northwest. Artificial recharge should prioritize the northwest despite declines from 15–19 m to 7–11 m (Sadeghi-Lari *et al*., 2024). Automated early warning systems should be established at high-RMSE locations (Scanlon *et al*., 2023), alongside quality-focused management in the southeast where saltwater intrusion persists. A dynamic extraction quota system based on seasonal projections should allow higher pumping during recharge periods (Rahmani *et al*., 2023), and areas with RMSE > 0.5 designated as high-risk zones. Community-based monitoring programs should enhance stakeholder engagement (Forliano *et al*., 2024; Kotir *et al*., 2024). These region-specific strategies achieve more sustainable groundwater management than uniform policies. Future research should incorporate real-time data, higher-resolution satellite observations, and physical constraints to reduce uncertainties (Rezk *et al*., 2024).

5. Conclusion

This study developed and evaluated a hybrid groundwater level (GWL) prediction framework using satellite-based data and three GMDH variants (GMDH, GMDH-GA, and GMDH-HS) across 15 observation wells in the Kahoorestan Plain, southern Iran, under three temporal scenarios (t, t+5, t+10). All models effectively captured temporal and spatial trends in groundwater levels, with the GMDH-HS model outperforming the others across all evaluation metrics (RMSE, EF, and R^2), achieving a 27–39% reduction in mean prediction error compared to standard GMDH and yielding R^2 values between 0.82 and 0.94. Spatial analysis revealed higher prediction accuracy in the northwestern region and greater challenges in saltwater intrusion areas. Critically, 10-year projections indicated a marked groundwater depletion trend, with eastern region levels predicted to drop 1.851 meters below the surface, signaling severe aquifer stress. These results support GMDH-HS as a strategic framework for groundwater monitoring and management in arid, data-scarce regions globally. The findings highlight the effectiveness of hybrid modeling approaches—particularly the integration of Harmony Search with GMDH—in improving long-term predictions, enabling local authorities to design proactive management strategies such as early warning systems and targeted recharge initiatives. Future studies would benefit from incorporating real-time hydrological and climatic data to further enhance temporal accuracy and account for sudden environmental changes.

Acknowledgments

The authors gratefully acknowledge the Regional Water Authority of Hormozgan Province for providing the observation well records used in this study. We also thank NASA's Jet Propulsion Laboratory (JPL) for making the GRACE gravity data publicly available, and the providers of the TRMM precipitation and satellite-derived soil moisture, temperature, and potential evapotranspiration datasets. The authors are further grateful to the University of Zabol and the University of Hormozgan for their institutional and technical support throughout this research.

Author Contributions

Jamshid Piri: Conceptualization, methodology, software, model development, writing—original draft. Adnan Sadeghi-Lari: Conceptualization, supervision, data curation, validation, writing—review and editing, project administration (corresponding author). Mohammad Kazemi: Formal analysis, investigation, resources, data curation. Narges Kariminejad: Visualization, trend analysis, writing—review and editing. All authors read and approved the final manuscript.

Funding

This research did not receive any specific grant from funding agencies in the public, commercial, or not-for-profit sectors.

Competing Interests

The authors declare that they have no known competing financial interests or personal relationships that could have appeared to influence the work reported in this paper.

Data Availability

The GRACE-JPL gravity data, TRMM precipitation data, and satellite-derived soil moisture, temperature, and potential evapotranspiration datasets used in this study are publicly available from their respective providers. The groundwater observation well records were obtained from the Regional Water Authority of Hormozgan Province and are available from the corresponding author upon reasonable request, subject to the data-sharing policies of the provider.
Two things to confirm: whether any grant actually funded this (the funding statement assumes none — change it if there was), and the exact CRediT roles per author, since I inferred those from the contribution patterns. The attached comment ([HJ1]) asks you to align all items with the journal's *Guide for Authors* — if you upload that file, I can match the exact wording and section order DESERT requires.

References

Adams, K. H., Reager, J. T., Rosen, P., Wiese, D. N., Farr, T. G., Rao, S., Haines, B. J., Argus, D. F., Liu, Z., & Smith, R. (2022). Remote sensing of groundwater: Current capabilities and future directions. *Water Resources Research*, *58*(10), Article e2022WR032219.

Bamal, A., Uddin, M. G., & Olbert, A. I. (2024). Harnessing machine learning for assessing climate change influences on groundwater resources: A comprehensive review. *Heliyon*, *10*(12), Article e32728.

Dodangeh, E., Panahi, M., Rezaie, F., Lee, S., Bui, D. T., Lee, C.-W., & Pradhan, B. (2020). Novel hybrid intelligence models for flood-susceptibility prediction: Meta optimization of the GMDH and SVR models with the genetic algorithm and harmony search. *Journal of Hydrology*, *590*, Article 125423.

Dube, T., Seaton, D., Shoko, C., & Mbow, C. (2023). Advancements in earth observation for water resources monitoring and management in Africa: A comprehensive review. *Journal of Hydrology*, *623*, Article 129738.

El Kenawy, A. M. (2024). Hydroclimatic extremes in arid and semi-arid regions: Status, challenges, and future outlook. In *Hydroclimatic extremes in the Middle East and North Africa* (pp. 1–22). Elsevier.

FatehiJananloo, M., Stopps, H., & McArthur, J. (2024). Exploring artificial intelligence methods for energy prediction in healthcare facilities: An in-depth extended systematic review. *Energy and Buildings*, *322*, Article 114598.

Forliano, C., De Bernardi, P., Rozsa, Z., & Bertello, A. (2024). Systems dynamics research in management and organization studies: Overview and research agenda. *Journal of Innovation & Knowledge*, *9*(3), Article 100512.

Ibrahim, A., Wayayok, A., Shafri, H. Z. M., & Toridi, N. M. (2024). Remote sensing technologies for modelling groundwater storage dynamics: Comprehensive review. *Journal of Hydrology X*, *22*, Article 100175.

Ivakhnenko, A. (2020). Past, present, and future of GMDH. In *Self-organizing methods in modeling* (pp. 105–119). CRC Press.

Khajeh, M., Ghaffari-Moghaddam, M., Piri, J., Barkhordar, A., & Ozturk, T. (2024). Machine learning-aided enhancement of white tea extraction efficiency using hybridized GMDH models in microwave-assisted extraction. *Scientific Reports*, *14*(1), Article 25900.

Kotir, J. H., Jagustovic, R., Papachristos, G., Zougmore, R. B., Kessler, A., Reynolds, M., Ouedraogo, M., Ritsema, C. J., Aziz, A. A., & Johnstone, R. (2024). Field experiences and lessons learned from applying participatory system dynamics modelling to sustainable water and agri-food systems. *Journal of Cleaner Production*, *434*, Article 140042.

Kumar, P., & Choudhury, D. (2024). Innovative technologies for effective water resources management. In *Water crises and sustainable management in the Global South* (pp. 555–594). Publisher Name.

Lubis, A. M., Fauzi, H. W., & Akbar, A. J. (2025). Groundwater potential assessment in Pino region, South Bengkulu, Indonesia using geo-investigation, remote sensing, and GIS approaches. *Results in Earth Sciences*, *3*, Article 100059.

Mukherjee, A., Scanlon, B. R., Aureli, A., Langan, S., Guo, H., & McKenzie, A. (2021). Global groundwater: From scarcity to security through sustainability and solutions. In A. Mukherjee, B. R. Scanlon, A. Aureli, S. Langan, H. Guo, & A. McKenzie (Eds.), *Global groundwater* (pp. 3–20). Elsevier.

Panahi, M., Rahmati, O., Rezaie, F., Lee, S., Mohammadi, F., & Conoscenti, C. (2022). Application of the group method of data handling (GMDH) approach for landslide susceptibility zonation using readily available spatial covariates. *Catena*, *208*, Article 105779.

Piri, J., Kahkha, M. R. R., & Kisi, O. (2024). Hybrid machine learning approach integrating GMDH and SVR for heavy metal concentration prediction in dust samples. *Environmental Science and Pollution Research*, *31*(12), 18230–18249.

Rahmani, M., Jahromi, S. H. M., & Darvishi, H. H. (2023). SD-DSS model of sustainable groundwater resources management using the water-food-energy security nexus in Alborz Province. *Ain Shams Engineering Journal*, *14*(1), Article 101812.

Rezk, H., Olabi, A. G., Mahmoud, M., Wilberforce, T., & Sayed, E. T. (2024). Metaheuristics and multi-criteria decision-making for renewable energy systems: Review, progress, bibliometric analysis, and contribution to the sustainable development pillars. *Ain Shams Engineering Journal*, *15*(8), Article 102883.

Sabangban, N., Panagant, N., Bureerat, S., Wansasueb, K., Kuma, S., Yildiz, A. R., & Pholdee, N. (2023). Simultaneous aerodynamic and structural optimisation of a low-speed horizontal-axis wind turbine blade using metaheuristic algorithms. *Materials Testing*, *65*(5), 699–714.

Sadeghi-Lari, A., Bahrami, M., & Dastandaz, T. (2024). Temporal and spatial variations of groundwater quantity and quality for drinking and irrigation purposes in the arid and hot weather of Southern Iran. *Physics and Chemistry of the Earth, Parts A/B/C*, *134*, Article 103582.

Safa, G., Najiba, C., El Houda, B. N., Monji, H., Soumaya, A., & Kamel, Z. (2020). Assessment of urban groundwater vulnerability in arid areas: Case of Sidi Bouzid aquifer (central Tunisia). *Journal of African Earth Sciences*, *168*, Article 103849.

Saha, A., & Pal, S. C. (2024). Application of machine learning and emerging remote sensing techniques in hydrology: A state-of-the-art review and current research trends. *Journal of Hydrology*, *632*, Article 130907.

Sajib, A. M., Bamal, A., Diganta, M. T. M., Ashekuzzaman, S., Rahman, A., Olbert, A. I., & Uddin, M. G. (2025). Novel groundwater quality index (GWQI) model: A reliable approach for the assessment of groundwater. *Results in Engineering*, *25*, Article 104265.

Scanlon, B. R., Fakhreddine, S., Rateb, A., de Graaf, I., Famiglietti, J., Gleeson, T., Grafton, R. Q., Jobbagy, E., Kebede, S., & Kolusu, S. R. (2023). Global water resources and the role of groundwater in a resilient water future. *Nature Reviews Earth & Environment*, *4*(2), 87–101.

Sengupta, S., Mohinuddin, S., Arif, M., Sengupta, B., & Zhang, W. (2022). Assessment of agricultural land suitability using GIS and fuzzy analytical hierarchy process approach in Ranchi District, India. *Geocarto International*, *37*(26), 13337–13368.

Shams, A. K., & Muhammad, N. S. (2023). Towards sustainable transboundary water cooperation between Afghanistan and Pakistan: A case study of Kabul River. *Ain Shams Engineering Journal*, *14*(2), Article 101842.

Springer, A., Lopez, T., Owor, M., Frappart, F., & Stieglitz, T. (2023). The role of space-based observations for groundwater resource monitoring over Africa. *Surveys in Geophysics*, *44*(1), 123–172.

Tao, H., Hameed, M. M., Marhoon, H. A., Zounemat-Kermani, M., Heddam, S., Kim, S., Sulaiman, S. O., Tan, M. L., Sa'adi, Z., & Mehr, A. D. (2022). Groundwater level prediction using machine learning models: A comprehensive review. *Neurocomputing*, *489*, 271–308.

Uddin, M. G., Rana, M. S. P., Diganta, M. T. M., Bamal, A., Sajib, A. M., Abioui, M., Shaibur, M. R., Ashekuzzaman, S., Nikoo, M. R., & Rahman, A. (2024). Enhancing groundwater quality assessment in coastal area: A hybrid modeling approach. *Heliyon*, *10*(13), Article e33345.

Xu, L., Bai, L., Xiao, J., Liu, Q., Chen, E., Wang, X., & Tang, Y. (2021). Multiple graph kernel learning based on GMDH-type neural network. *Information Fusion*, *66*, 100–110.

Yeh, H.-F., Cheng, Y.-S., Lin, H.-I., & Lee, C.-H. (2016). Mapping groundwater recharge potential zone using a GIS approach in Hualian River, Taiwan. *Sustainable Environment Research*, *26*(1), 33–43.

Zhou, W., Yan, Z., & Zhang, L. (2024). A comparative study of 11 non-linear regression models highlighting autoencoder, DBN, and SVR, enhanced by SHAP importance analysis in soybean branching prediction. *Scientific Reports*, *14*(1), Article 5905.